NASA TECHNICAL NOTE

NASA TN D-7834

NASA TN D-7834

APPLICATION OF A PARAMETER IDENTIFICATION TECHNIQUE TO A HINGELESS HELICOPTER ROTOR

by Gerd Kanning and James C. Biggers

Ames Research Center

Moffett Field, Calif. 94035

NATIONAL AERONAUTICS AND SPACE ADMINISTRATION • WASHINGTON, D. C. • DECEMBER 1974

1. Report No.	2. Government Accession No.	3. Recipient's Catalog No.
NASA TN D-7834		

4. Title and Subtitle	5. Report Date
APPLICATION OF A PARAMETER IDENTIFICATION TECHNIQUE TO A HINGELESS HELICOPTER ROTOR	December 1974
	6. Performing Organization Code

7. Author(s)	8. Performing Organization Report No.
Gerd Kanning and James C. Biggers	A-5289
	10. Work Unit No. 760-63-01

9. Performing Organization Name and Address	11. Contract or Grant No.
NASA Ames Research Center Moffett Field, Calif. 94035	
	13. Type of Report and Period Covered
12. Sponsoring Agency Name and Address	Technical Note
National Aeronautics and Space Administration Washington, D. C. 20546	14. Sponsoring Agency Code

15. Supplementary Notes

16. Abstract

A mathematical model of a gyro-controlled, three-bladed hingeless helicopter rotor was developed and parameters of the model were estimated using a parameter identification technique. The flapping and feathering degrees of freedom of the blades were modeled. The equations of the model contain time-varying, periodic coefficients due to the forward speed of the rotor. A digital simulation of the analytical model was compared with wind-tunnel measurements to establish the validity of the model. Comparisons of steady-state and transient solutions of the analytical model with the tunnel measurements gave reasonably good matching of gyro angle but less satisfactory matching of hub moment measurements. Further improvements were obtained by use of a parameter identification technique to adjust as many as 10 parameters of the analytical model. The sensitivity of the blade response to small changes in the parameters was also calculated. The most sensitive parameters were found to be collective pitch, blade twist, tip loss factor, blade to gyro coupling constant, Lock number, and equivalent flapping hinge spring constant.

17. Key Words (Suggested by Author(s))	18. Distribution Statement
Helicopter parameter identification Helicopter rotor modeling Mathematical modeling Helicopters Modeling Identification	Unclassified - Unlimited Cat. 02

19. Security Classif. (of this report)	20. Security Classif. (of this page)	21. No. of Pages	22. Price*
Unclassified	Unclassified	68	$3.00

*For sale by the National Technical Information Service, Springfield, Virginia 22151

TABLE OF CONTENTS

SYMBOLS

$\bar{A}(t)$	time-varying matrix defined in appendix D (table 1)
a	lift-curve slope equal to 6.28
B	frame formed by vectors $(\bar{b}_1,\bar{b}_2,\bar{b}_3)$ which defines the blade frame
B_ℓ	tip loss factor
b	number of blades
$(\bar{b}_1,\bar{b}_2,\bar{b}_3)$	orthogonal unit vectors defined as the B frame
C	frame formed by vectors $(\bar{c}_1,\bar{c}_2,\bar{c}_3)$ which defines the gyro cage frame
$\bar{C}$	transformation matrix between state variables and measurement
C_2	coupling constant between blade and angular displacement of gyro
C_D	drag coefficient, $\frac{D}{(1/2)\rho V^2 \pi R_b^2}$
C_L	lift coefficient, $\frac{L}{(1/2)\rho V^2 \pi R_b^2}$
$C1(\psi),C2(\psi),C3(\psi),C4(\psi),C5(\psi),C6(\psi),C7(\psi)$	defined by equation (A35)
C_s	damping constant for nonrotating part of swashplate, Nm/rad/sec (ft-lb/rad/sec)
C_T	thrust coefficient, $\frac{T}{\pi R^2 \rho (\Omega R_b)^2}$
c	blade chord, m (ft)
c_ℓ	defined by equation (A20)
c_n	defined by equation (A20)
$(\bar{c}_1,\bar{c}_2,\bar{c}_3)$	orthogonal unit vectors defined as the C frame
c_θ	damping constant about feathering axis (rotating axis), Nm/rad/sec (ft-lb/rad/sec)

D	drag, N (lb)
$\left(\frac{d}{dt}\right)_S$	time rate of change with respect to inertial space
e	hinge offset, m (ft)
F_{β_X}	force at hub in rotating coordinates along X axis, N (lb)
F_{β_Y}	force at hub in rotating coordinates along Y axis, N (lb)
FWD	forward direction
$\bar{f}(t)$	column vector of forcing functions for rotor equations
G	frame formed by vectors $(\bar{g}_1,\bar{g}_2,\bar{g}_3)$ which defines the gyro frame
G_{RPM}	rotational speed of gyro, rpm
$(\bar{g}_1,\bar{g}_2,\bar{g}_3)$	orthogonal unit vectors defined as the G frame
$\bar{H}_G$	angular momentum of gyro, Nm^2/sec ($slug\text{-}ft^2/sec$)
h_{LC}	distance from hub to load cell moment sensor, m (ft); $\bar{h}_{LC} = (0,0,h_{LC_z})$
h_s	distance from hub to location of shaft moment sensor, m (ft); $\bar{h}_s = (0,0,h_{s_z})$
I_D	diametric moment of inertia of gyro, $kg\text{-}m^2$ ($slug\text{-}ft^2$)
$\bar{\bar{I}}_G$	gyro inertia matrix defined by equation (B13), $kg\text{-}m^2$ ($slug\text{-}ft^2$)
I_{GE}	equivalent inertia of gyro $I_D + 1.5C_2^2I_x$, $kg\text{-}m^2$ ($slug\text{-}ft^2$)
I_3	polar moment of inertia of gyro, $kg\text{-}m^2$ ($slug\text{-}ft^2$)
I_x,I_y,I_z	inertia characteristics of blade, $kg\text{-}m^2$ ($slug\text{-}ft^2$)
K_s	stationary spring constant for swashplate, Nm/rad (ft-lb/rad)
$K1,B2,B3,B4,B5$	defined by equation (A34)
k_R	ratio of gyro angular velocity to rotor angular velocity
k_β	spring constant of blade, Nm/rad (ft-lb/rad); $k_\beta = I_y\Omega^2\left[p^2 - 1 - \frac{(3/2)e}{R_b-e} - \frac{\gamma}{8}\tan\delta_3\right]$

k_θ spring constant about feathering axis, Nm/rad (ft-lb/rad)

L lift, N (lb)

M_{exc} excitation of the gyro by the blade in the R frame along X_r, Nm (ft-lb)

$M_{exc_{xc}}$ x-component of M_{exc} in C frame, Nm (ft-lb)

$M_{exc_{yc}}$ y-component of M_{exc} in C frame, Nm (ft-lb)

M_{G_x} applied moment to gyro along X in the C frame, Nm (ft-lb)

M_{G_y} applied moment to gyro along Y in the C frame (Nm (ft-lb)

M_{LC_x} load cell roll moment in stationary coordinates measured 0.914 m (3 ft) below hub, Nm (ft-lb)

M_{LC_y} load cell pitch moment in stationary coordinates measured 0.914 m (3 ft) below hub, Nm (ft-lb)

M_x moment about X axis in the B frame

M_y moment about Y axis in the B frame

$M_{y_{aero}}$ aerodynamic moment about flapping axis, Nm (ft-lb)

$M_{x_{inertia}}$ inertia moment about feathering axis, Nm (ft-lb)

$M_{y_{inertia}}$ inertia moment about flapping axis, Nm (ft-lb)

$M_{x_{mech}}$ mechanical moment about feathering axis, Nm (ft-lb)

$M_{y_{mech}}$ mechanical moment about flapping axis, Nm (ft-lb)

M_{x_s} hub moment in stationary coordinates (left roll positive), Nm (ft-lb)

M_{y_s} hub moment in stationary coordinates (nose-up positive), Nm (ft-lb)

M_{x_r} shaft bending moment about X_r axis 0.369 m (0.917 ft) below hub, Nm (ft-lb)

M_{y_r} shaft bending moment about Y_r axis 0.369 m (0.917 ft) below hub, Nm (ft-lb)

M_{β_x} roll moment at hub in rotating coordinates (positive left roll), Nm (ft-lb)

M_{β_y} pitch moment at hub in rotating coordinates (positive nose-up), Nm (ft-lb)

n	nth blade
p	ratio of flapping natural frequency to rotor frequency $\frac{\omega}{\Omega}$
q	dynamic pressure, $\frac{\rho V^2}{2}$, N/m^2 (lb/ft^2)
R	frame formed by vectors $(\bar{r}_1,\bar{r}_2,\bar{r}_3)$ which defines the shaft axis system rotating at rotor speed
R_b	blade radius, m (ft)
r	distance along blade from center of rotation, m (ft)
$(\bar{r}_1,\bar{r}_2,\bar{r}_3)$	orthogonal unit vectors defined as the R frame
S	frame formed by vectors $(\bar{s}_1,\bar{s}_2,\bar{s}_3)$ which defines the stationary axis system of the rotor; also referred to as the inertial frame
$(\bar{s}_1,\bar{s}_2,\bar{s}_3)$	orthogonal unit vectors defined as the S frame
T	rotor thrust, N (lb)
t	time, sec
U_R,U_T,U_P	radial, tangential, and perpendicular wind velocity components, m/sec (ft/sec)
$\bar{u}$	input vector
V	airspeed, m/sec (ft/sec)
X,Y,Z	right-handed coordinate system with the positive X axis aft over helicopter tail section and the positive Z axis pointing up
x	ratio of radial distance to blade radius, $\frac{r}{R_b}$
$\bar{x}$	state variable
$\bar{y}$	measurement vector
$\alpha = \theta-\phi$	angle between relative wind and blade chord axis - angle of attack, deg
α_s	angle of attack of hub plane
β	flapping angle of blade (positive up), deg
β_p	precone angle, deg

$\beta_1, \beta_2, \beta_3$ flapping angles of blades 1, 2, and 3, deg

γ Lock number, $\gamma = \frac{c\rho a R_b^4}{I_y}$

δ_3 pitch flap coupling, deg

δ_1 gyro angle, left roll positive, rotating coordinates, deg

δ_2 gyro angle, nose-up positive, rotating coordinates, deg

ζ lag angle of blade, deg

ζ_o blade sweep angle, deg

θ feathering angle of blade, deg

θ_o collective pitch, deg

θ_1 blade twist, deg

θ_{cyc} cyclic pitch angle, deg

θ_{sp} swashplate pitch angle, positive nose-up (stationary coordinates), deg

$\theta_1, \theta_2, \theta_3$ feathering angles of blades 1, 2, and 3, deg

θ_{1C} cyclic pitch, nose up at $\psi = 0$, deg

θ_{1S} cyclic pitch, nose up at $\psi = 90^\circ$, deg

λ inflow positive up, $\lambda_o + \lambda_x x \cos \psi + \theta_y x \sin \psi$

μ advance ratio, $\frac{V \cos \alpha_s}{R_b}$

ν_1 swashplate roll moment input (stationary coordinates, positive left roll), Nm (ft-lb)

ν_2 swashplate pitch moment input (stationary coordinates, positive nose-up), Nm (ft-lb)

ρ air density, kg/m^3 ($slug/ft^3$)

ϕ inflow angle, deg

ϕ_{sp} swashplate roll angle, positive left roll, stationary coordinates, deg

ψ azimuth angle measured in direction of rotation, deg

ψ_o	pitch link angle, deg (see fig. 3)
Ω	angular velocity of rotor, rad/sec
ω	blade flapping natural frequency, rad/sec
ω_G	gyro angular velocity, rad/sec
$\omega_x, \omega_y, \omega_z$	angular velocities of blade defined by equation (A3), rad/sec
$\omega_{C/R}$	angular velocity of C frame with respect to R frame, rad/sec
$\omega_{C/S}$	angular velocity of C frame with respect to inertial space, rad/sec
$\omega_{G/C}$	angular velocity of G frame with respect to C frame, rad/sec
$\omega_{R/S}$	angular velocity of R frame with respect to inertial space, rad/sec

APPLICATION OF A PARAMETER IDENTIFICATION TECHNIQUE TO A HINGELESS HELICOPTER ROTOR

Gerd Kanning and James C. Biggers

Ames Research Center

SUMMARY

A mathematical model of a three-bladed hingeless rotor with a high-speed gyro in the feathering system was developed and parameters of the model were estimated using a parameter identification technique. The flapping degree of freedom of each blade was modeled by assuming the existence of a virtual hinge near the hub. The feathering degree of freedom was modeled in conjunction with the motion of the gyro. The gyro prescribed the feathering sequence to each of the blades. In the aerodynamic moment terms, the reverse velocity effect of the retreating blades was included. The complete gyro and rotor equations contain time-varying periodic coefficients due to the forward speed of the rotor. A digital simulation of these equations was obtained to generate steady-state and transient solutions of the mathematical model. For steady-state operation, with the gyro inoperative, the model response was matched quite accurately to the measured data by adjusting selected model parameters with a parameter identification technique. For transient operation, with the rotor controlled by the gyro, considerably larger hub moments were calculated than measured while calculated gyro angles were in reasonable agreement with measured gyro angles. Application of the parameter identification technique resulted in improved hub moment matching when as many as 10 parameters of the model were adjusted simultaneously. The sensitivity of the blade response to small changes in the parameters was also calculated. The most sensitive parameters were found to be collective pitch, blade twist, tip loss factor, blade to gyro coupling constant, Lock number, and equivalent flapping hinge spring constant.

INTRODUCTION

The application of parameter identification techniques to the problem of estimating stability derivatives for fixed-wing aircraft has been reported by many investigators (refs. 1, 2, and 3). These techniques have been applied to helicopters more recently (refs. 4 and 5). In reference 4, stability and control derivatives were estimated from helicopter flight data; in reference 5, the feasibility of estimating specific parameters contained in a rotor math model was investigated. The results of reference 5 indicate that good estimates of the parameters can be obtained with identification techniques. However, in reference 5, the math model itself was used to generate the data used in the identification procedure. This provides a check on the parameter identification algorithm, but provides no information concerning the validity

of the math model itself. This limitation is removed in this report by use of data obtained in the wind tunnel for the identification procedure.

A gyro-controlled hingeless helicopter rotor has been tested in the Ames 40- by 80-Foot Wind Tunnel. The rotor blades were relatively stiff with an undamped natural flapping frequency of about 1.25 cycles/rev at 100 percent RPM. An expository analysis of this rotor system is given in references 6 and 7 where calculated cyclic angles for trimming rotor hub and swashplate moments were compared with experimental data at high advance ratios (> 0.5). Vibratory loads on the same rotor at high advance ratios were studied in reference 8. The mathematical model used in the above three references contains simplifying assumptions that are valid only for high advance ratios. The mathematical model developed here is valid for advance ratios below 0.5. Although the wind-tunnel tests were aimed at the slowed-stopped operation of the rotor and therefore emphasized high advance ratios, some data were obtained for advance ratios less than 0.5. These latter data were used for parameter identification in refining the parameters of the math model of the rotor. In the math model, each blade of the rotor was allowed flapping and feathering degrees of freedom independent of the others. The first blade flapping mode was represented by rigid blade motion about a spring-restraint virtual hinge. The blades were also swept forward by an angle ζ_0 from the feathering axis, allowing flapping moments to be fed back into the feathering axis and hence to the control gyro.

The behavior of the mathematical model for different inputs was investigated by integrating the time-varying periodic differential equations forward for several rotor revolutions. The simulation was compared with wind-tunnel data during both steady-state and transient conditions. Steady-state and transient responses for advance ratios up to 0.40 were used in the comparison. Parameters of the model such as blade inertia, flapping hinge spring constant, blade to gyro coupling constant, Lock number, tip loss factor, collective pitch, and blade sweep angle were systematically varied using a parameter identification technique to give the best match between the simulation and the wind-tunnel measurements. The sensitivity of these parameters on the output response was also calculated.

DEVELOPMENT OF THE ANALYTICAL MODEL

An analytical model was developed for a three-bladed hingeless rotor with a high-speed gyro in the feathering system (fig. 1). A list of assumptions and the derivation of the equations are given in appendices A and B. The complete rotor equations are derived as follows. First, the equations for the blade motion are obtained; the equations for the gyro and gyro-blade interaction are then derived; and, finally, these two sets of equations are combined to yield the complete set.

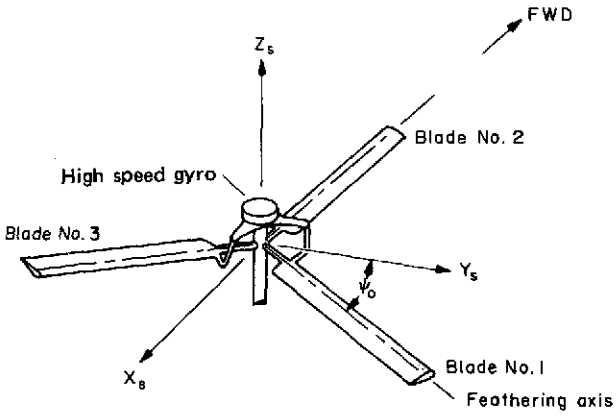

Figure 1.- Gyro-controlled hingeless rotor.

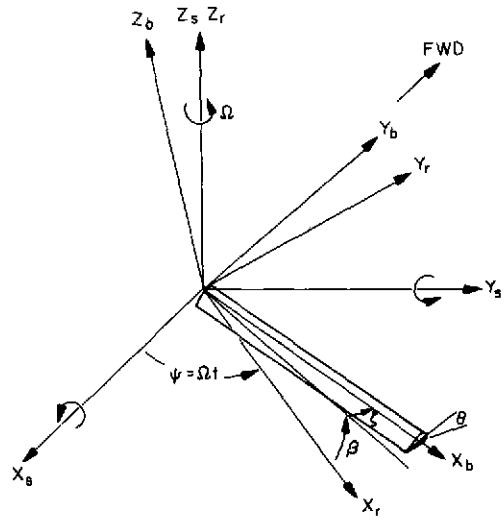

Figure 2.- Rotor-blade coordinate system.

Blade Equations

The equations for the flapping and feathering motion are obtained by writing the moment equilibrium about the hub. Figure 2 shows the coordinate system used in writing the moment equilibrium. The X_s, Y_s, Z_s coordinates represent the stationary axis system with the X_s axis rearward over the tail section of the helicopter, the Y_s axis to the right, and the Z_s axis upward. The positive direction of rotation about each stationary axis is indicated in the figure. The azimuth angle ψ is measured positive from the stationary axis X_s in the direction of rotor rotation. The positive direction of the flapping angle β, inplane angle ζ, and feathering angle θ is also shown in figure 2. The effects of the inplane motion are included in the equations derived in appendix A. However, for the verification and discussions in this report, the equations are simplified by fixing the inplane deflection at ζ_o, the preset blade sweep angle. This simplification is reasonable if resonance of the ζ motion is avoided (ref. 6). The moments acting about the hinge point are the inertial, aerodynamic, and mechanical moments. Each of these moments for the flapping degree of freedom is developed in this section. For the feathering degree of freedom, the equations are developed in conjunction with the gyro equations in appendices A and B because the feathering axis is mechanically connected to the gyro system. The inertia moment about the flapping axis is derived in appendix A (eq. (A13)):

$$M_{y_{inertia}} = I_y\ddot{\beta} - (I_x + I_y\zeta_o^2 - I_z)\Omega^2\beta + \frac{3}{2} I_y \frac{e}{R_b - e}\Omega^2\beta$$

$$-(I_x + I_y - I_z)\Omega\dot{\theta} - (I_z - I_y)\zeta_o\Omega^2\theta \qquad (1)$$

The aerodynamic moment about the flapping axis is also derived in appendix A. For linear aerodynamics with no stall effects included, the aerodynamic moment is written in abbreviated form (eq. (A36)) as

$$M_{y_{aero}} = -K1\{-C2(\psi)\dot{\beta} + [-C1(\psi) + C4(\psi)\tan\delta_3]\beta + C3(\psi)\theta_1 + C4(\psi)\theta_o + C4(\psi)\theta_{cyc} + C5(\psi)\lambda_o + C6(\psi)\lambda_x + C7(\psi)\lambda_y\} \quad (2)$$

The coefficients of equation (2), defined by equations (A34) and (A35), are repeated here for completeness:

$$K1 = \frac{\gamma I_y \Omega^2}{2}$$

$$B2 = \frac{B^2}{2} - \frac{e^2}{2R_b^2}$$

$$B3 = \frac{B^3}{3} - \frac{e^3}{3R_b^3}$$

$$B4 = \frac{B^4}{4} - \frac{e^4}{4R_b^4}$$

$$B5 = \frac{B^5}{5} - \frac{e^5}{5R_b^5}$$

$$C1(\psi) = \zeta_o B4 + \mu(\cos\psi + \zeta_o \sin\psi)B3 + \frac{1}{2}\mu^2(\zeta_o + \zeta_o \cos 2\psi + \sin 2\psi)B2$$

$$C2(\psi) = \frac{B4}{\Omega} + \frac{\mu}{\Omega}(\zeta_o \cos\psi + \sin\psi)B3$$

$$C3(\psi) = B5 + 2\mu(\zeta_o \cos\psi + \sin\psi)B4 + \mu^2\left(\frac{1}{2} - \frac{1}{2}\cos 2\psi + \zeta_o \sin 2\psi\right)B3$$

$$C4(\psi) = B4 + 2\mu(\zeta_o \cos\psi + \sin\psi)B3 + \mu^2\left(\frac{1}{2} - \frac{1}{2}\cos 2\psi + \zeta_o \sin 2\psi\right)B2$$

$$C5(\psi) = B3 + \mu(\zeta_o \cos\psi + \sin\psi)B2$$

$$C6(\psi) = B4 \cos\psi + \mu(\cos\psi \sin\psi + \zeta_o \cos^2\psi)B3$$

$$C7(\psi) = B4 \sin\psi + \mu(\sin^2\psi + \zeta_o \cos\psi \sin\psi)B3$$

The reverse flow region encountered by the retreating blade during forward flight was modeled in the aerodynamic moment term of equation (2). The reverse flow region was approximated by assuming that reverse flow existed

from an azimuth 225° to 315° and from the root $x = \mu$. The appropriate changes required in the coefficients of the aerodynamic moment equation (2) are given in appendix A.

The other moment component is produced by the spring restraint of the blade at the hub. For the flapping axis, this moment is given by $k_\beta(\beta-\beta_p)$, where k_β represents the spring constant of the blade and $(\beta-\beta_p)$ represents the flapping deflection away from the precone position.

The mechanical spring moment for the flapping axis can be written as (eq. (A37)):

$$M_{y_{mech}} = k_\beta(\beta - \beta_p) \tag{3}$$

The moment equilibrium about the flapping axis is now given by the sum of the inertia, aerodynamic, and mechanical moments. The flapping equation may be written by combining equations (1), (2), and (3) to form:

$$M_{y_{inertia}} + M_{y_{aero}} + M_{y_{mech}} = 0$$

which gives

$$I_y\ddot{\beta} - (I_x + I_y\zeta_o^2 - I_z)\Omega^2\beta + \frac{3}{2} I_y \frac{e}{R_b-e} \Omega^2\beta - (I_x + I_y - I_z)\Omega\dot{\theta} - (I_z - I_y)\zeta_o\Omega^2\theta$$

$$-K1\{-C2(\psi)\dot{\beta} + [-C1(\psi) + C4(\psi)\tan\delta_3]\beta + C3(\psi)\theta_1 + C4(\psi)\theta_o + C4(\psi)\theta_{cyc}$$

$$+C5(\psi)\lambda_o + C6(\psi)\lambda_x + C7(\psi)\lambda_y\} + k_\beta(\beta - \beta_p) = 0 \tag{4}$$

Equation (4) describes the flapping motion of each blade and will be used later to develop equations for a three-bladed rotor.

Gyro Equations

The gyro of the rotor system modeled prescribes a feathering sequence to the blades. The equations for the gyro are developed about its axes system and the relationship of the feathering axes with the gyro is then established. The coordinates used to derive the gyro equations are shown in figure 3. The coordinates X_s,Y_s,Z_s and X_r,Y_r,Z_r are the stationary and rotating coordinates of the blade as previously defined. The X_c,Y_c,Z_c coordinates define the rotating coordinates of the gyro. The equations for the gyro are obtained by expanding the angular momentum equation $[d\bar{H}_G/dt]_S = \bar{M}_G$. This equation is expanded in appendix B. In terms of the gyro coordinates δ_1 and δ_2, the equations for the gyro are (eqs. (B25) and (B26)):

$$I_G\ddot{\delta}_1 + (I_3\Omega^2k_R - I_G\Omega^2)\delta_1 + (I_3\Omega k_R - 2\Omega I_G)\dot{\delta}_2 - \Omega C_s\delta_2 + C_s\dot{\delta}_1 + K_s\delta_1 - M_{exc_{xc}}$$
$$= \nu_1\sin(\psi+\psi_o) - \nu_2\cos(\psi+\psi_o) \tag{5}$$

$$I_G\ddot{\delta}_2 + (I_3\Omega^2k_R - I_G\Omega^2)\delta_2 - (I_3\Omega k_R - 2\Omega I_G)\dot{\delta}_1 + \Omega C_s\delta_1 + C_s\dot{\delta}_2 + K_s\delta_2 - M_{exc_{yc}}$$
$$= \nu_1\cos(\psi+\psi_o) + \nu_2\sin(\psi+\psi_o) \tag{6}$$

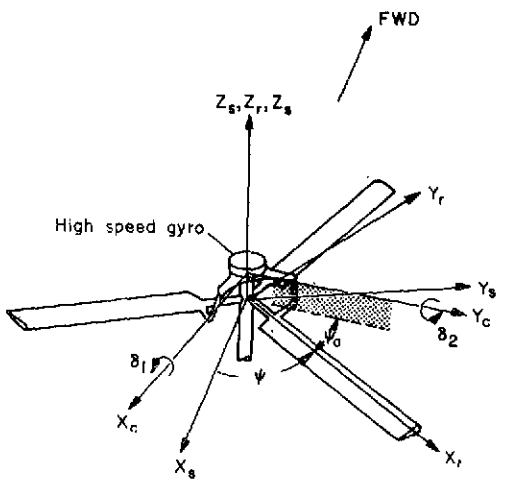

Figure 3.- Gyro coordinates.

The left sides of the equations represent the inertial properties of the gyro, the spring and damper effects (K_s,C_s) about the δ_1 and δ_2 axes, and the excitation of the gyro by the blades ($M_{exc_{xc}}$ and $M_{exc_{yc}}$). The right side of the equations represent the roll (ν_1) and pitch (ν_2) moment inputs of the pilot. The pilot input is via a moment (not displacement) applied to the gyro in the nonrotating frame. The gyro responds to the input moment as well as to moments applied by the blades. The $M_{exc_{xc}}$ and $M_{exc_{yc}}$ terms in equations (5) and (6) are the moments applied by the blades and must now be obtained from the feathering equations of the blade expressed in the gyro axes system. The moments contributing to the excitation are the blade inertia and mechanical moments about the feathering axis. Aerodynamic moments about the feathering axis are assumed negligible. In addition, flapping moments coupling into the feathering axis due to the forward sweep of the blade must also be included. The complete moment expression in the blade frame, given by equation (B27), is expanded by substituting the appropriate moments and then expressing the moment equation in the gyro axis system. The excitation of the gyro by the blade expanded for a three-bladed rotor and transformed to the X_c,Y_c coordinates is given as (eqs. (B31) and (B32)):

$$M_{exc_{xc}} = C_2\Big\{-I_x\Big(\ddot{\theta}_1 - \tfrac{1}{2}\ddot{\theta}_2 - \tfrac{1}{2}\ddot{\theta}_3\Big) - c_\theta\Big(\dot{\theta}_1 - \tfrac{1}{2}\dot{\theta}_2 - \tfrac{1}{2}\dot{\theta}_3\Big) - (I_z-I_y)\Omega^2\Big(\theta_1 - \tfrac{1}{2}\theta_2$$
$$- \tfrac{1}{2}\theta_3\Big) - k_\theta\Big(\theta_1 - \tfrac{1}{2}\theta_2 - \tfrac{1}{2}\theta_3\Big) - (I_x+I_y-I_z)\Omega\Big(\dot{\beta}_1 - \tfrac{1}{2}\dot{\beta}_2 - \tfrac{1}{2}\dot{\beta}_3\Big) + (I_z-I_y)$$
$$\times\zeta_o\Omega^2\Big(\beta_1 - \tfrac{1}{2}\beta_2 - \tfrac{1}{2}\beta_3\Big) + \zeta_o k_\beta\Big[(\beta_1-\beta_p) - \tfrac{1}{2}(\beta_2-\beta_p) - \tfrac{1}{2}(\beta_3-\beta_p)\Big]\Big\} \tag{7}$$

$$M_{exc_{yc}} = \frac{\sqrt{3}}{2} C_2\{-I_x(\ddot{\theta}_2-\ddot{\theta}_3) - c_\theta(\dot{\theta}_2-\dot{\theta}_3) - (I_z-I_y)\Omega^2(\theta_2-\theta_3) - k_\theta(\theta_2-\theta_3)$$
$$-(I_x+I_y-I_z)\Omega(\dot{\beta}_2-\dot{\beta}_3) + (I_z-I_y)\zeta_o\Omega^2(\beta_2-\beta_3) + \zeta_o k_\beta[(\beta_2-\beta_p) - (\beta_3-\beta_p)]\} \tag{8}$$

The gyro equations are now obtained by combining equations (7) and (8) with (5) and (6) and transforming the feathering angle θ for each blade and their derivatives to gyro coordinates. The transformation between θ_1, θ_2, θ_3 and δ_1, δ_2 is given by (eq. (A40)):

$$\theta_i = C_2\left[\delta_1\cos(i-1)\frac{2\pi}{b} + \delta_2\sin(i-1)\frac{2\pi}{b}\right]; \quad i = 1, \ldots, b \tag{9}$$

where $b = 3$. Substituting the above transformation and its derivatives into equations (7) and (8) gives the complete gyro equations for a three-bladed rotor (eqs. (B35) and (B36)):

$$\left(I_G+\frac{3}{2}C_2^2I_x\right)\ddot{\delta}_1+\frac{3}{2}c_\theta C_2^2\dot{\delta}_1+C_s\dot{\delta}_1+(I_3\Omega^2k_R-I_G\Omega^2)\delta_1+\frac{3}{2}C_2^2(I_z-I_y)\Omega^2\delta_1+\frac{3}{2}k_\theta C_2^2\delta_1+K_s\delta_1$$
$$+(I_3\Omega k_R-2\Omega I_G)\dot{\delta}_2-\Omega C_s\delta_2+C_2(I_x+I_y-I_z)\Omega\left(\dot{\beta}_1-\frac{1}{2}\dot{\beta}_2-\frac{1}{2}\dot{\beta}_3\right)-C_2(I_z-I_y)\zeta_o\Omega^2$$
$$\times\left(\beta_1-\frac{1}{2}\beta_2-\frac{1}{2}\beta_3\right)-C_2\zeta_o k_\beta\left[(\beta_1-\beta_p)-\frac{1}{2}(\beta_2-\beta_p)-\frac{1}{2}(\beta_3-\beta_p)\right]$$
$$= \nu_1\sin(\psi+\psi_o)-\nu_2\cos(\psi+\psi_o) \tag{10}$$

$$\left(I_G+\frac{3}{2}C_2^2I_x\right)\ddot{\delta}_2+\frac{3}{2}c_\theta C_2^2\dot{\delta}_2+C_s\dot{\delta}_2+(I_3\Omega^2k_R-\Omega^2I_G)\delta_2+\frac{3}{2}C_2^2(I_z-I_y)\Omega^2\delta_2+\frac{3}{2}k_\theta C_2^2\delta_2+K_s\delta_2$$
$$-(I_3\Omega k_R-2\Omega I_G)\dot{\delta}_1+\Omega C_s\delta_1+\frac{\sqrt{3}}{2}C_2(I_x+I_y-I_z)\Omega(\dot{\beta}_2-\dot{\beta}_3)-\frac{\sqrt{3}}{2}C_2(I_z-I_y)\zeta_o\Omega^2(\beta_2-\beta_3)$$
$$-\frac{\sqrt{3}}{2}C_2\zeta_o k_\beta[(\beta_2-\beta_p)-(\beta_3-\beta_p)] = \nu_1\cos(\psi+\psi_o)+\nu_2\sin(\psi+\psi_o) \tag{11}$$

Rotor Equations

The flapping equation (4) was written for one blade. For the three-bladed rotor, the flapping angle β and the feathering angle are subscripted 1, 2, and 3; for the azimuth angle ψ in equation (4), the substitution of ψ, $\psi+120°$, and $\psi+240°$ for each blade must be made, respectively. The flapping equation can then be written as

$$I_y\ddot{\beta}_i-(I_x+I_y\zeta_o^2-I_z)\Omega^2\beta_i+\frac{3}{2}I_y\frac{e}{R-e}\Omega^2\beta_i-(I_x+I_y-I_z)\Omega\dot{\theta}_i-(I_z-I_y)\zeta_o\Omega^2\theta_i$$

$$-K1\left\{-C2\left[\psi+(i-1)\frac{2\pi}{b}\right]\dot{\beta}-C1\left[\psi+(i-1)\frac{2\pi}{b}\right]\beta_i+C4\left[\psi+(i-1)\frac{2\pi}{b}\right]\beta_i\tan\delta_3+C3\left[\psi+(i-1)\frac{2\pi}{b}\right]\theta_1\right.$$

$$\left.+C4\left[\psi+(i-1)\frac{2\pi}{b}\right](\theta_o+\theta_{cyc})+C5\left[\psi+(i-1)\frac{2\pi}{b}\right]\lambda_o+C6\left[\psi+(i-1)\frac{2\pi}{b}\right]\lambda_x+C7\left[\psi+(i-1)\frac{2\pi}{b}\right]\lambda_y\right\}$$

$$+k_\beta(\beta_i-\beta_p)=0 \qquad i=1,\ 2,\ 3 \qquad (12)$$

The feathering angle θ and its derivatives in equation (12) are written in gyro coordinates (see eq. (9)). In appendix A, the transformation equation (9) has been applied to equation (12) to convert the feathering angles to gyro angles. The equations for each blade are given in expanded form by equations (A41), (A42), and (A43). The gyro equations with the feathering equations interconnected for the three blades were written in gyro coordinates in the previous section. The complete set of rotor equations is now given by the two gyro equations (10) and (11) and the blade equations from equation (12) for $i = 1, 2$, and 3.

Method of Solution and Transformation of Equations to Measurement Coordinates

In this section, the transformation to measurement coordinates is discussed, followed by a description of the method for calculating time histories from the math model.

The five equations discussed in the previous section (eqs. (10) and (11) and eq. (12) for $i = 1, 2, 3$) are next written in first-order form for the digital simulation. The first-order state variables are defined as follows:

$$\begin{bmatrix} x_1 \\ x_2 \\ x_3 \\ x_4 \\ x_5 \\ x_6 \\ x_7 \\ x_8 \\ x_9 \\ x_{10} \end{bmatrix} = \begin{bmatrix} \delta_1 \\ \dot{\delta}_1 \\ \delta_2 \\ \dot{\delta}_2 \\ \beta_1 \\ \dot{\beta}_1 \\ \beta_2 \\ \dot{\beta}_2 \\ \beta_3 \\ \dot{\beta}_3 \end{bmatrix} \qquad (13)$$

Applying these transformations of state variables to the five rotor equations gives the equations of the rotor in the form $\dot{\bar{x}} = \bar{A}(t)\bar{x} + \bar{f}(t)$ (see table 1). The equations were integrated using the Runge-Kutta, fixed stepwise integration routine. The output of the integration process produced flapping angles and gyro angles. However, flapping angles could not be measured during the wind-tunnel tests; hub moments were recorded instead. Therefore, a transformation was required to convert the flapping angles to hub moments. The transformation from moments to flapping angles, derived in appendix C (eqs. (C12) and (C13)), is given below:

$$M_{\beta_x} = k_\beta\left(\frac{1}{2}\sqrt{3}\,\beta_2 - \frac{1}{2}\sqrt{3}\,\beta_3\right) \tag{14}$$

$$M_{\beta_y} = k_\beta\left(-\beta_1 + \frac{1}{2}\beta_2 + \frac{1}{2}\beta_3\right) \tag{15}$$

where the shearing force at the hinge was considered small since the rotor was lightly loaded. Equations (14) and (15) were written in the form $\bar{y} = \bar{C}\bar{x}$, where $\bar{y}$ is the vector of moments and $\bar{x}$ is the vector of flapping angles. The complete set of rotor equations ($\dot{\bar{x}} = \bar{A}(t)\bar{x} + \bar{f}(t)$ and $\bar{y} = \bar{C}\bar{x}$) in first-order form is shown in table 1.

The simulation and measurement results were both performed in the rotating coordinate frame X_r, Y_r, Z_r (shown in fig. 2). During the analysis of the data, it was found in some instances that the hub moments and angles could be better understood if the moments and angles were transformed to a nonrotating coordinate frame at the hub center - the X_s, Y_s, Z_s frame discussed previously (fig. 2). The transformations between these reference frames are also given in appendix C.

BEHAVIOR OF SIMULATION MODEL

Parameters of Model

The nominal values of the parameters for the rotor and the gyro used in the analytical model simulation are given in table 2. These parameters were obtained by direct measurement or calculation.

The first flapping mode of the blade was represented by rigid blade motion about a spring restraint virtual hinge located a distance e radially from the hub center. The spring constant about this virtual hinge was calculated from

$$k_\beta = I_y\Omega^2\left(p^2 - 1 - \frac{3}{2}\frac{e}{R_b - e} - \frac{\gamma}{8}\tan\delta_3\right) \tag{16}$$

where

I_y blade flapping inertia

Ω rotor angular velocity

p flapping natural frequency to rotor frequency

e virtual hinge location

R_b blade radius

γ Lock number

δ_3 pitch flap coupling angle

However, for this rotor, δ_3 was zero and the spring constant was evaluated from the first three terms of equation (16). The values for p in equation (16) were obtained from reference 6 and are given as a function of percent rotor RPM in figure 4. The values for I_y, Ω, and R_b were obtained by measurement, while the virtual hinge location e was found to be between 11 to 15 percent of the blade radius (to be discussed later). The variation of spring constant with percent rotor RPM with I_y = 363.4 kg-m^2 (268 slug-ft^2), δ_3 = 0, and e/R_b = 0.11 is also shown in figure 4.

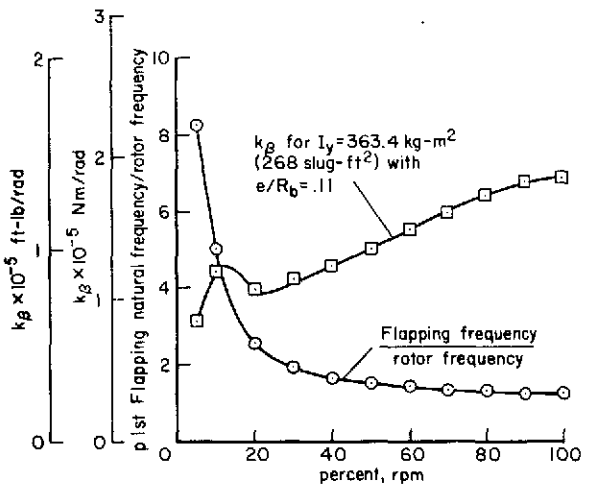

Figure 4.- Blade flapping frequency ratio and blade spring constant as a function of percent rotor RPM (100-percent RPM = 355.6).

Time Response

The rotor flapping response for different inputs was investigated by integrating the time-varying periodic differential equations forward for several rotor revolutions. The parameters in the math model used to generate these time histories are given in table 2 and those unique to the particular case studied are given with the results in each figure. The virtual hinge location was fixed at 11 percent of the blade radius to illustrate the model behavior. First, the response of the rotor in hover was obtained. Figure 5(a) shows the blade flapping angles before and after a step input of 2° was applied to the collective control at the start of the second rotor revolution. The gyro angles and the hub moments are zero since the swashplate moment inputs were taken as zero for this run. The transient motion of the blade flapping angles is shown for about one rotor revolution (fig. 5(a)) after which the coning angle reaches a new steady-state value. Figure 5(b) shows the response of the rotor in hover but with an incremental step swashplate roll moment input of $M_{\phi_{sp}}$ = 27 Nm (20 ft-lb) applied at the second rotor revolution ($M_{\phi_{sp}}$ = 41 Nm (30 ft-lb) before the step input). The swashplate pitch moment and the collective pitch angle were held fixed at $M_{\phi_{sp}}$ = -14 Nm

(-10 ft-lb) and $\theta_o = 8.57°$, respectively. For this case, with moments applied to the gyro, the hub moments are not zero. The transient response of hub moments in rotating coordinates (R-frame), gyro angles, and blade flapping angles are shown in figure 5(b).

Two additional transient responses were calculated but for the rotor in forward flight with advance ratios of $\mu = 0.212$ and 0.485 (figs. 6 and 7). Figure 6 shows the transient response of the blade flapping angles, gyro angles, and hub moments for a step moment input applied about the swashplate roll axis. The first two rotor revolutions in figure 6 show the steady-state behavior with $M_{\phi_{sp}} = 41$ Nm (30 ft-lb), $M_{\phi_{sp}} = -14$ Nm (-10 ft-lb), and $\theta_o = 8.57°$. At the second rotor revolution, an incremental step input about the swashplate roll axis of 27 Nm (20 ft-lb) was applied while the swashplate pitch moment and collective pitch angle remained the same. The transient motion that followed is shown from the second to the eighth rotor revolution.

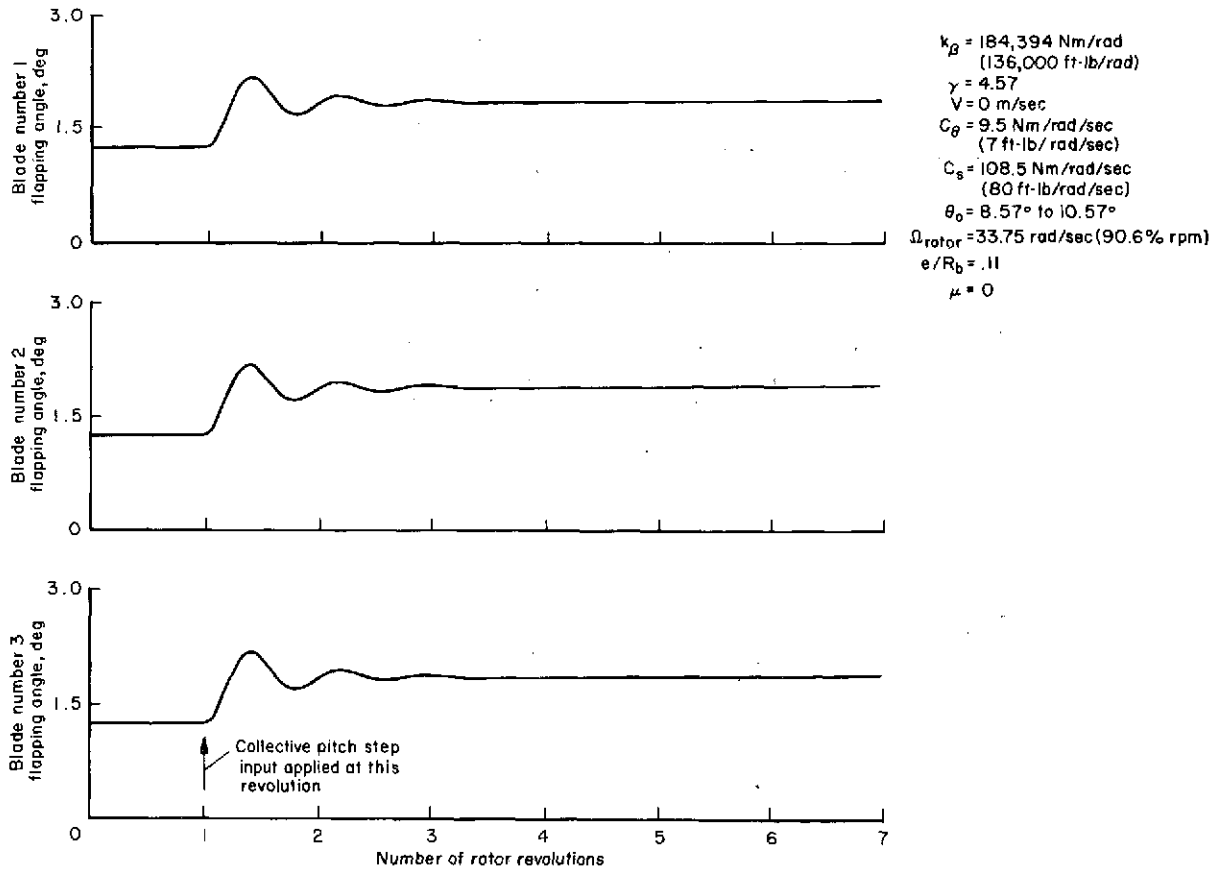

(a) Response to a step collective pitch input at the start of the second rotor revolution.

Figure 5.- Transient response at hover.

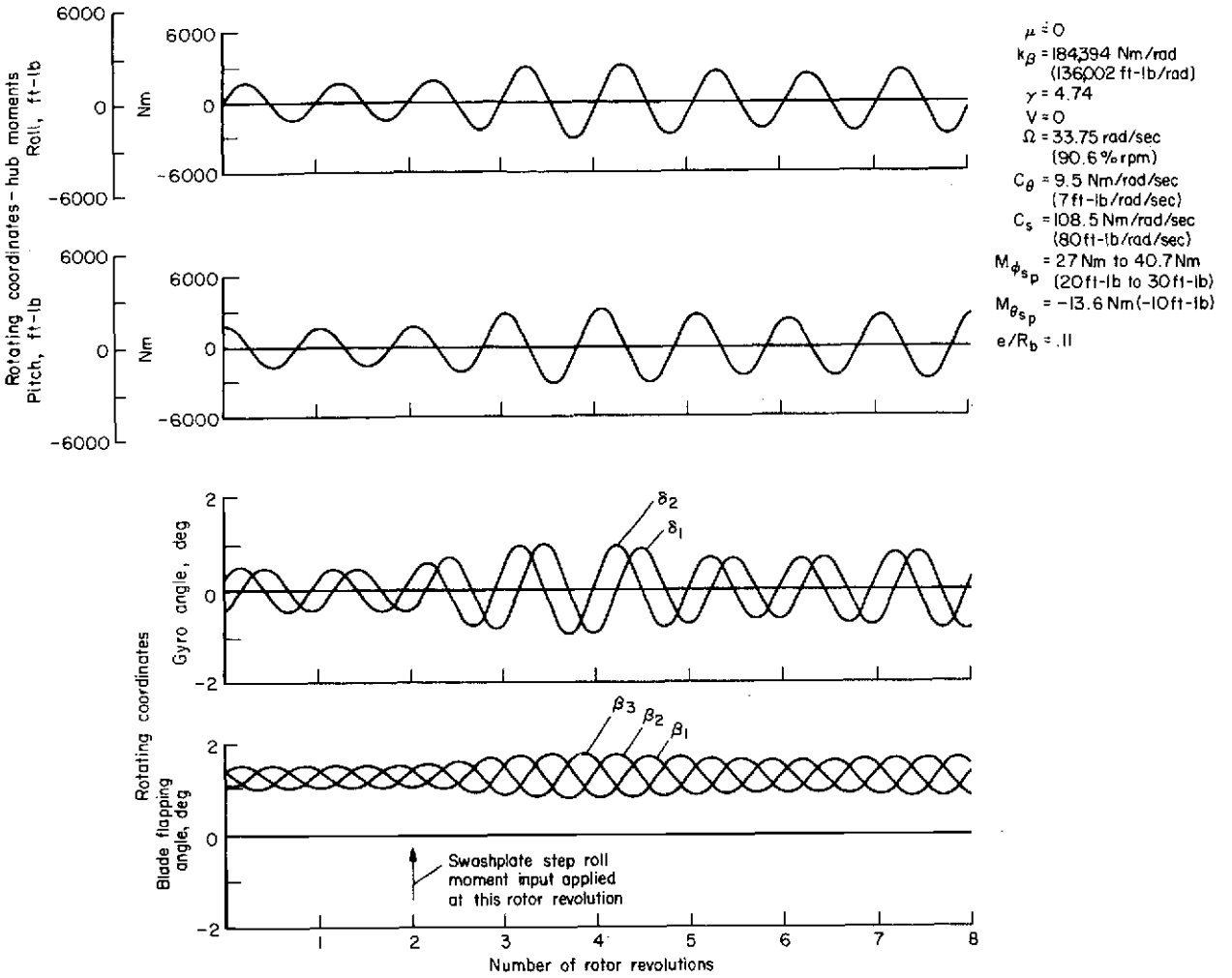

(b) Response to a swashplate roll moment input at the start of the third rotor revolution.

Figure 5.- Concluded.

In like manner, the same swashplate inputs were applied as when the rotor was operating at an advance ratio of $\mu = 0.485$ (fig. 7). A comparison of the transient behavior of the rotor at the two different advance ratios indicates that for the lower advance ratio the response is sinusoidal, whereas for the higher advance ratio the response shows the presence of higher harmonic terms. This effect is due to the periodic terms in the differential equations which become significant at the higher advance ratios.

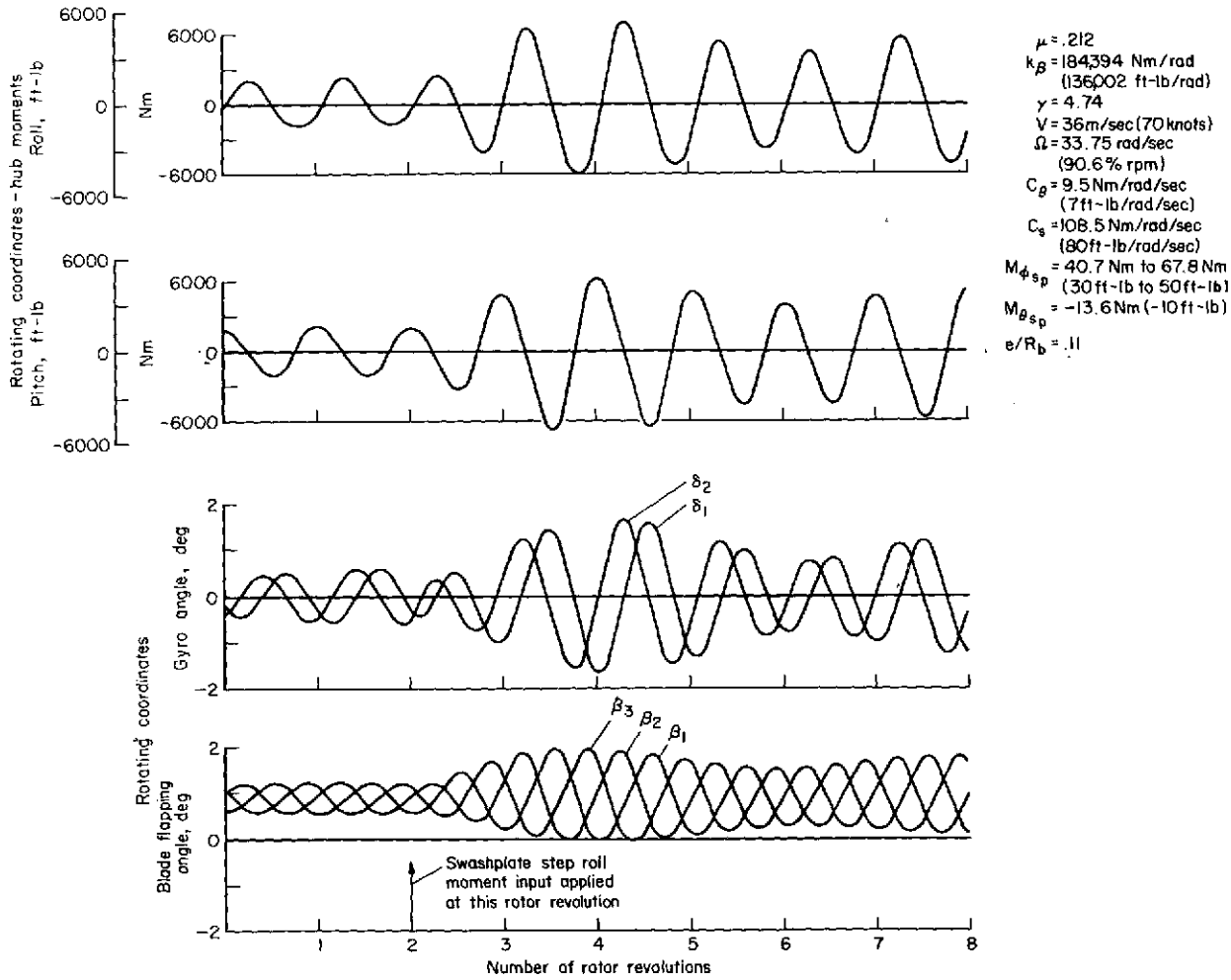

Figure 6.- Transient response to a swashplate roll moment input at the start of the third rotor revolution for $\mu = 0.212$.

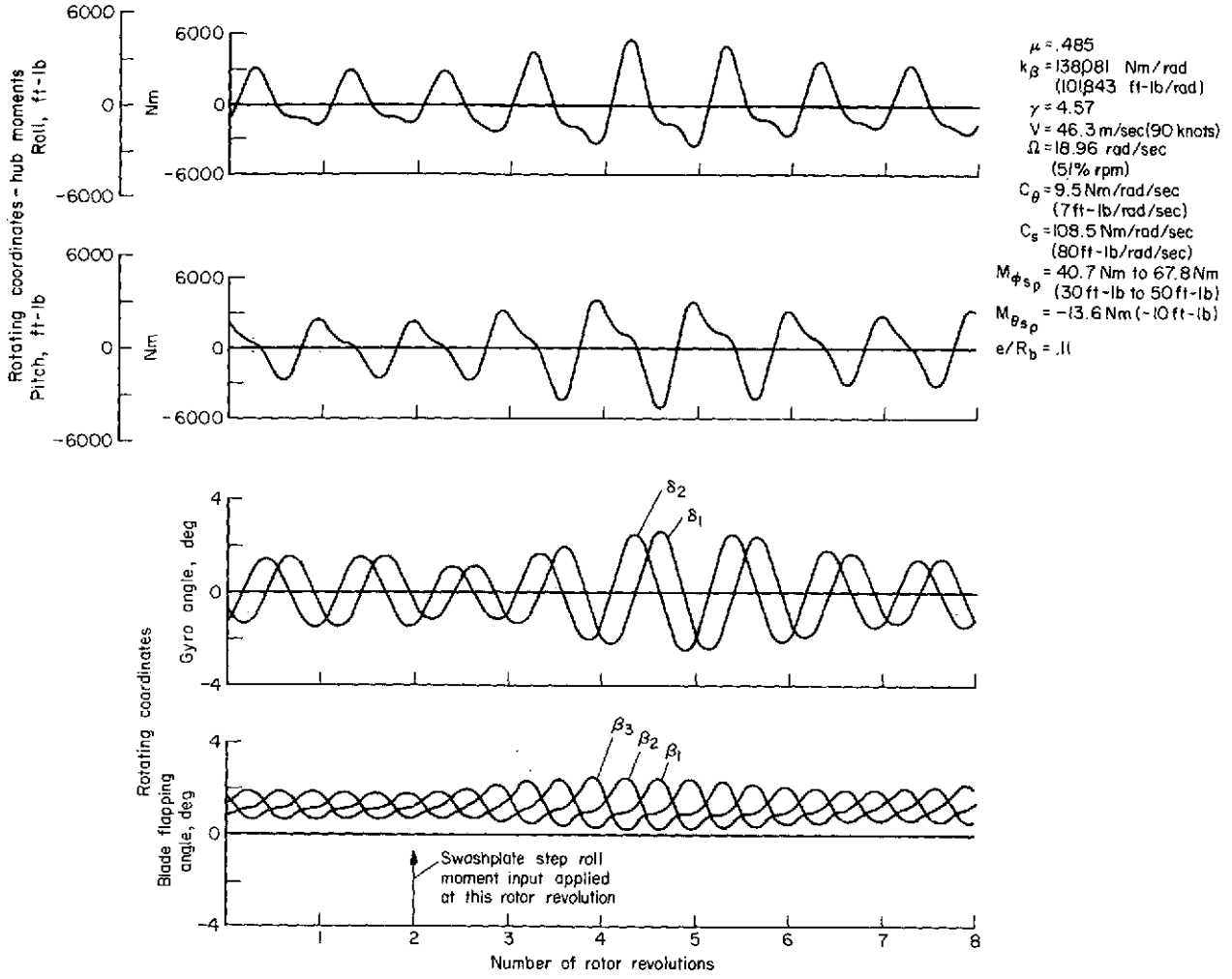

Figure 7.- Transient response to a swashplate roll moment input at the start of the third rotor revolution for $\mu = 0.485$.

APPLICATION OF PARAMETER IDENTIFICATION TECHNIQUE

The parameter identification process is useful in redesigning and refining the parameters of the math model using wind-tunnel or flight measurements. The parameters to be determined are those that appear in the coefficients of the differential equations, such as inertia, spring constant, Lock number, and damping constant. The general outline of the identification process is sketched in figure 8. The same input $\bar{u}$ is applied to both the math model and the plant ("plant" refers to the helicopter rotor test in the wind tunnel). The best values of the parameters of the math model are those that minimize the difference between the model and plant outputs ($\hat{y}$ and $\bar{y}$). The identification process is an algorithm that compares the outputs of the math model and plant and adjusts the parameter values (inertia, spring constant,

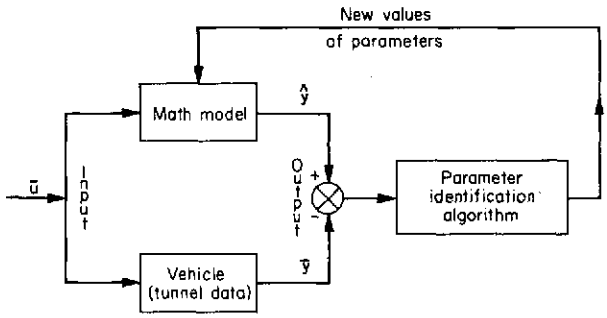

Figure 8.- Block diagram of parameter identification technique.

damping, etc.) until this difference is a minimum. What this minimum should be is established by least-squares fit within the limits of table 2, and the identification algorithm iterates until this criterion is reached. It may not always be possible to reach this minimum or even to obtain an improvement in the matching of the model and plant outputs. This report does not address these problems, but will make use of the technique in obtaining, where possible, a better match between the simulation and the measured data. For a detailed discussion of the parameter identification theory as applied here, see reference 9.

The identification program had the capability of identifying as many as 36 parameters of the mathematical model. For the results that follow, 6, 7, and 10 parameter cases were studied. The choice of parameters was based on the accuracy to which the parameters were known, the sensitivity of the parameters in affecting the response, and whether the parameters were linearly independent. The accuracy to which the parameters were known a priori established lower and upper bounds of variation for each parameter. A sensitivity analysis of all parameters indicated which ones were most sensitive in affecting the response. The linear independence or uniqueness of the parameters calculated by the identification program is discussed in detail in reference 9. Thus the parameters studied here were chosen on the basis of a priori knowledge, sensitivity, and linear independence. Tables 3 and 4 present the parameters identified and their nominal values obtained from reference 6.

The computation time required to identify more than 10 parameters over several rotor revolutions is large. The approximate time required to estimate one parameter using one measured data point per iteration was found to be about 1/20 of a second on an IBM 360/70 computer. This time could vary considerably since the computation time is not a linear relationship of the parameters estimated. Adequate reconstruction of the measured waveforms for parameter identification purposes could be achieved by sampling the data every 15° in azimuth. The integration step size was allowed to become no larger than 2°. In some cases, a larger step size could be used, but the 2° step size was found to be satisfactory in eliminating significant error accumulation when the equations are integrated for several rotor revolutions.

COMPARISON OF MEASURED AND SIMULATED DATA

Discussion of Measured Data

The measured data used to check the analytical model were obtained in the Ames 40- by 80-Foot Wind Tunnel for a three-bladed, hingeless rotor with a gyro coupled to the blade feathering axis. Figure 9 is a photograph of the model in the wind-tunnel test section. This model was used to investigate the behavior of the rotor under slowed-stopped conditions. For these conditions, the rotor was operated near zero lift. Hence the measurements taken during tunnel testing are for a lightly loaded rotor at relatively high advance ratios. The following measurements were recorded: load cell moments (moments in stationary coordinates 0.914 m below the hub), shaft bending moments, swashplate moments and angles, and blade angles. Data were available to check the analytical model and to identify parameters at forward speeds from about 31 to 41 m/sec (61 to 80 knots) and rotor RPM from 148 to 197. A complete description of the test and data collected is given in reference 6. For the steady-state cases used to check the analytical model, the rotor was operated in a locked gyro mode. For this mode, the swashplate was held fixed at specified angles while the rotor flapping angles were allowed to come to a steady-state condition. The transient data had been recorded by taking the

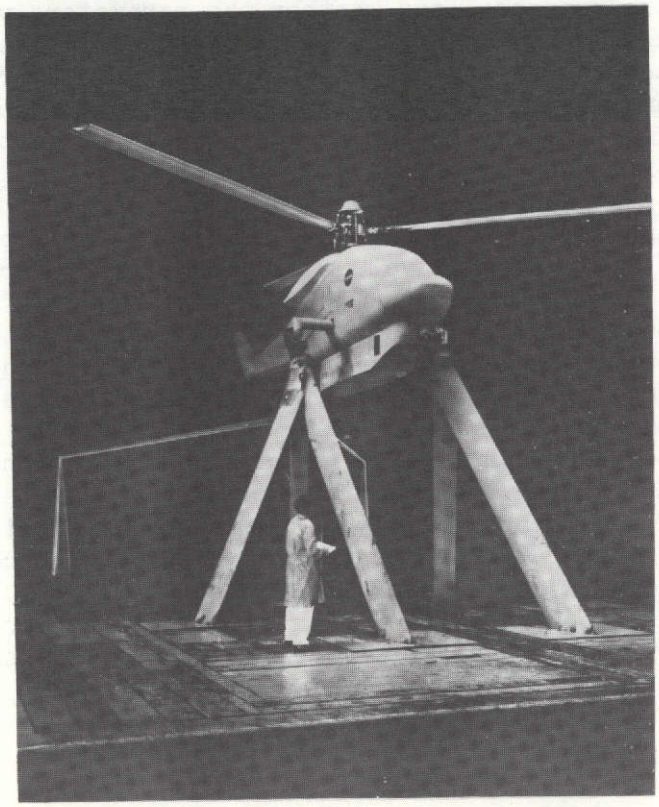

Figure 9.- Experimental rotor rig in the Ames 40- by 80-Foot Wind Tunnel.

rotor out of trim and then allowing it to return to a trim condition. This procedure amounted to a step change in the swashplate angle. The purpose of this procedure was to establish the rotor transient independent of gyro motion.

After the measured data were digitized and converted to engineering units, it became apparent that some filtering of the data was necessary. A low-pass digital filter with a corner frequency of 16 Hz was used to process the transient data. The low-pass filter eliminated some of the high-frequency noise and vibrations from the measured data without introducing any noticeable phase shift for frequencies of interest here. Figure 10 compares the filtered and unfiltered data for a typical transient run to show the quality of the data and the results of filtering.

In comparing the digital simulation with the measured data, care had to be taken to use the correct initial conditions in the model simulation. The initial conditions required for the computer simulation were gyro and flapping angles and rates and the moments applied to the swashplate. Since only

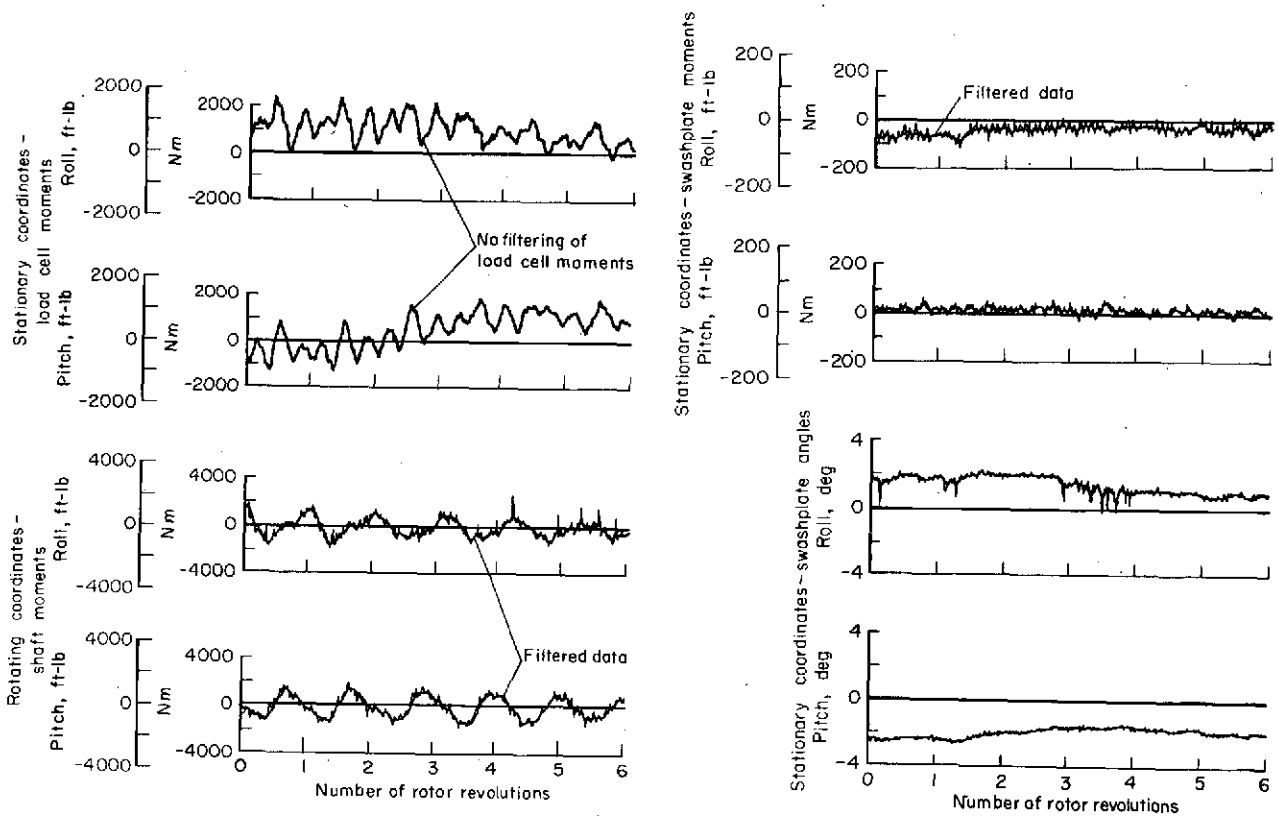

Figure 10.- Typical measured transient data with and without filtering; $\mu = 0.355$, $V = 36$ m/sec (70 knots).

gyro angles and swashplate moments had been recorded for each record taken in the wind tunnel, the gyro rates and flapping angles and rates had to be established. The gyro rates and the flapping angles and rates were obtained by entering into the computer simulation the known values of swashplate angles, rates, and moments and integrating the equations to steady-state conditions. The flapping angles and rates thus obtained served as the initial conditions for the particular tunnel record compared.

The next section presents steady-state and transient runs for different forward velocities and results obtained by applying the parameter identification program to the measured wind-tunnel data. For a steady-state condition, the gyro was held at a fixed attitude (locked gyro mode). For the transient run, the gyro was free to move but under the influence of moment inputs to the swashplate.

Steady-State Case: Locked Gyro

Figures 11 and 12 compare measured (discrete points) and simulated (solid line) hub moments for two different forward velocities but with about the same advance ratio. The main difference between these two cases is in p, the dimensionless flapping frequency. The rotor was operated in a locked gyro mode while the measured hub moments were recorded. In like manner, the mathematical model simulation was forced with the gyro angles and moments recorded during tunnel testing while the hub moments were allowed to vary. The nominal values used in the simulation are given in figures 11 and 12 for a virtual hinge e located at 11 percent of the blade radius. The math model shows similar waveforms for the hub moments without the presence of higher harmonics in the measured data. The vehicle moments are the 1/rev moments in rotating coordinates and these moments are important in controlling the vehicle. The higher harmonics seen in the measured data are associated with the vibratory modes of the vehicle. An amplitude difference in the math model results is apparent for both advance ratios studied. The largest difference in amplitude occurs for lower forward velocity with $\mu = 0.402$ and $p = 1.62$ (fig. 12).

The parameter identification program was applied and a number of parameters were adjusted simultaneously to improve the hub moment match. The results of the hub moment matching obtained after 10 parameters of the math model were identified are shown in figures 13 and 14, with the nominal values and estimated parameters for each case shown in tabular form. The inflow, uniform for both cases, was calculated from equation (A31). The spring constant of the blade was decreased from the nominal value. The ratio of hinge offset to blade radius (e/R_b) was allowed to vary and was found to be at 11 percent of the blade radius. The remaining parameters varied from 2 to 3 percent, which was the accuracy to which these parameters were known a priori. Improvement in the hub moment match is shown in figure 13 after the parameters were varied from their nominal value. The large difference between the measured and math model results for $\mu = 0.402$ (fig. 12) was considerably reduced as shown in figure 14. A comparison of the identified parameters, for the two steady-state cases studied, shows similar values of those

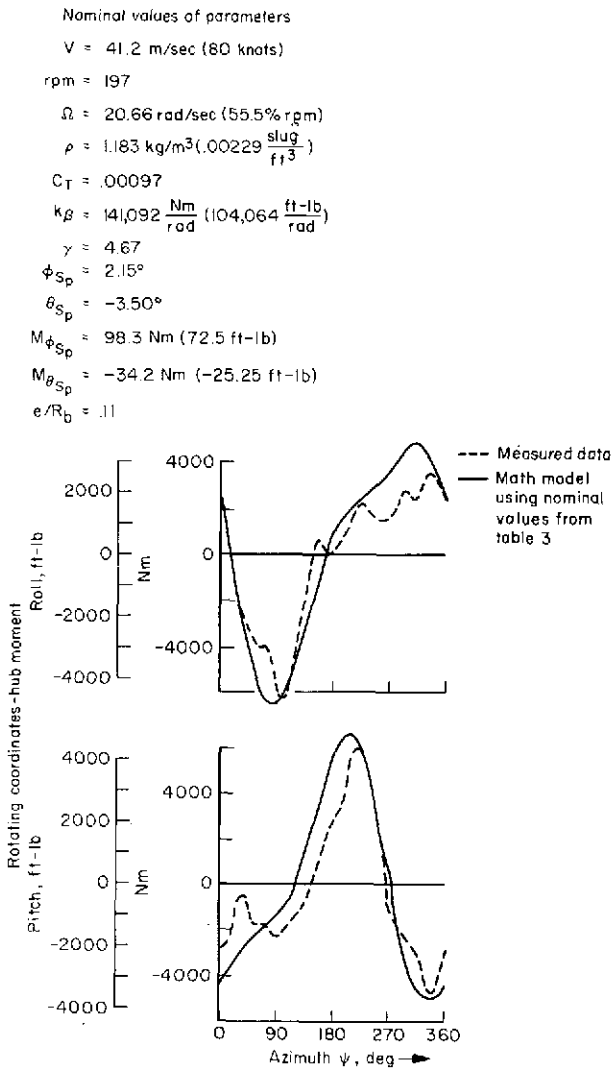

Figure 11.- Measured and simulated hub moments in rotating coordinates; μ = 0.399, p = 1.45.

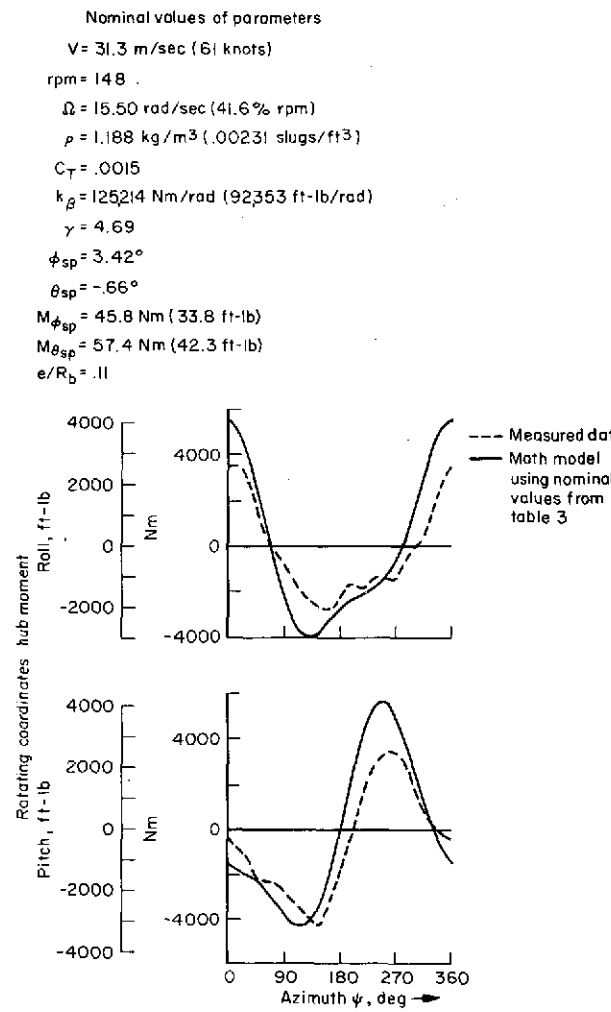

Figure 12.- Measured and simulated hub moments in rotating coordinates; μ = 0.402, p = 1.62.

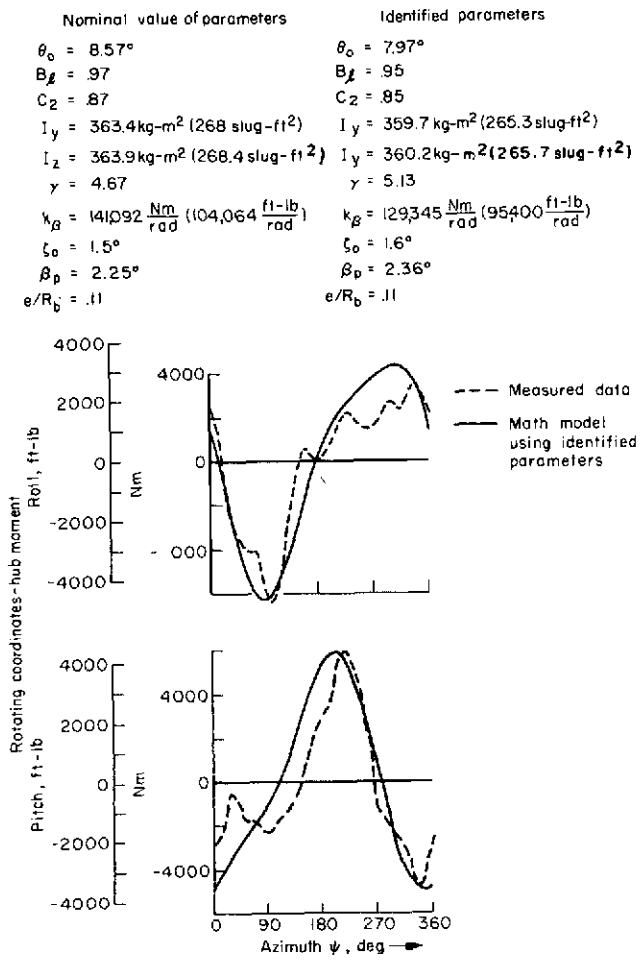

Figure 13.- Measured and identified hub moments - uniform inflow; $\mu = 0.399$, $p = 1.45$.

parameters allowed to vary. The inertia, tip loss factor, Lock number, blade sweep angle, collective pitch, gyro coupling constant, and hinge offset were the same after the identification for the two steady-state cases studied.

Transient Case: Free Gyro

In this section, the math model simulation output is compared with a transient run recorded during wind-tunnel testing. In addition, the parameter identification algorithm was again applied to improve the matching of simulated and measured data.

The transient measurements were recorded with the rotor operating in a free gyro mode and with a step roll moment applied about the swashplate roll axis. For the free gyro mode of operation, the gyro is free to move in response to moments from the blades and swashplate. The step input applied

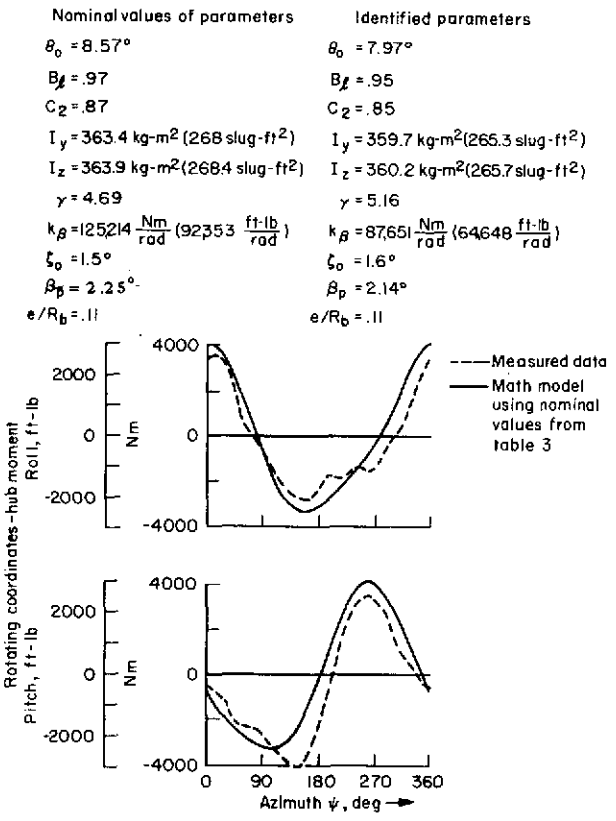

Figure 14.- Measured and identified hub moments - uniform inflow; μ = 0.402, p = 1.62.

to the roll axis of the swashplate was accomplished by taking the rotor out of trim and then moving the swashplate roll moment control quickly back to a trim position. The transient run was obtained at a forward velocity of 36 m/sec (70 knots) with a rotor speed of 192 RPM. The measured data had been filtered (discussed earlier) to eliminate the high-frequency components found on some of the recorded data. The nominal values of the parameters used in the math model simulation are shown in table 2. Those parameters unique for this advance ratio are tabulated in the figures next to the measured response.

The measured response (discrete points) of swashplate roll and pitch moments, hub moments, and gyro angles is shown in figure 15. The mathematical model response (solid line) of hub moments and gyro angles is superimposed on the measured data. Both measured and calculated hub moments and gyro angles are presented in rotating coordinates. The swashplate roll and pitch moment inputs used as forcing functions in the mathematical model simulation are shown in the upper two traces of figure 15. The step change of the swashplate roll moment is seen at the end of the third rotor revolution while the swashplate pitch moment remained unchanged. The initial conditions were obtained by forcing the math model with the swashplate inputs prior to the step change in the swashplate roll moment. Integrating the equations with these swashplate inputs until steady state was reached produced the initial conditions required to start the math model simulation. With these initial conditions, the measured and simulated time responses for this step swashplate roll moment input are shown in the lower four records of figure 15. Note that the gyro angles from the math model simulation match the measured data fairly closely. However, the magnitude of the hub moments is considerably different for the simulated data compared to the measured data.

Several identification runs were made so that a different set of parameters could be identified to improve moment and angle matching. Figure 16 shows the matching of hub moments and angles when six parameters of the math model were allowed to vary. Each parameter was allowed to vary over a percentage range from their nominal values. The percentage variation was

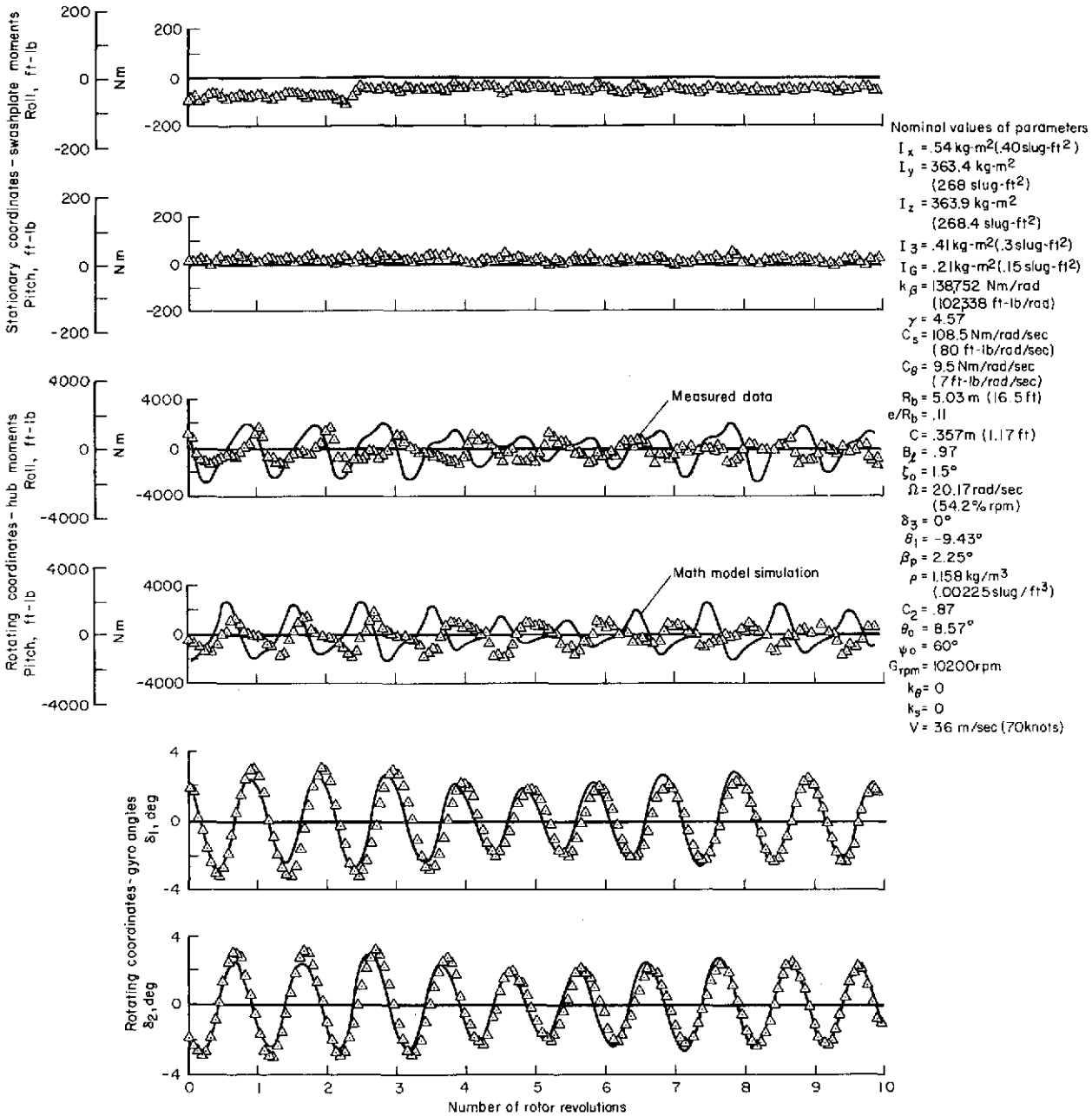

Figure 15.- Comparison of math model simulation with measured data, $\mu = 0.355$.

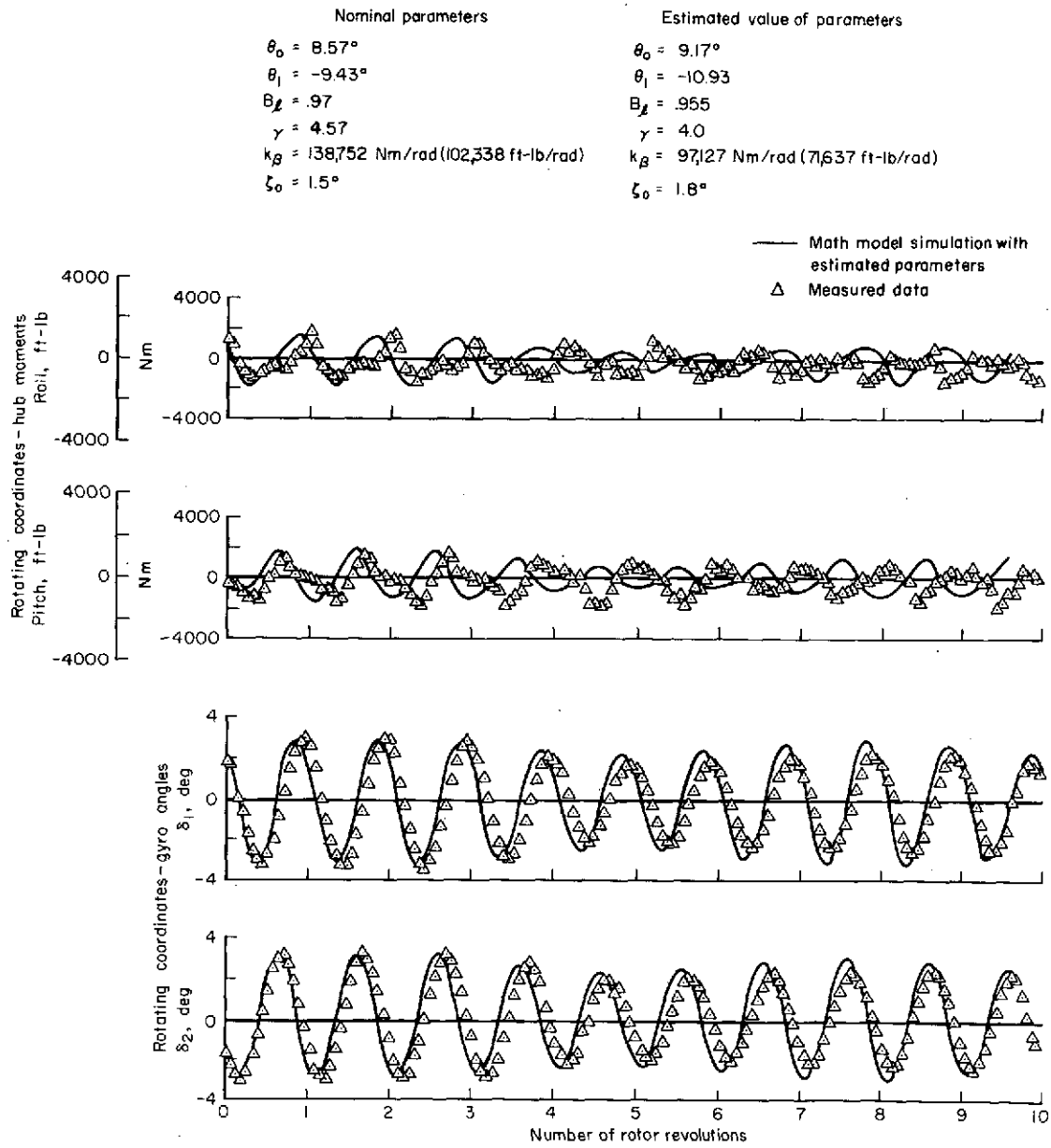

Figure 16.- Comparison of math model simulation with measured data using six estimated parameters, $\mu = 0.355$.

established from the accuracy with which these parameters were known a priori (table 2). Most parameters were known between 2 and 5 percent, although some (such as virtual hinge location and spring constant) were known far less accurately and therefore were allowed to vary over a large range. The hub moment matching was considerably improved after only a few iterations, while the angle matching remained about the same. The phase relation of the hub moments between the calculated and measured data did not improve. The parameters that gave a better match of the time histories are also shown in figure 16.

Figure 17 shows the matching obtained when seven parameters were allowed to vary. In this case, all parameters were the same as in the previous case except for the blade twist, which was held fixed while the flapping inertia and hinge offset were additional parameters that could be adjusted. The match of hub moments is not too different from the previous case. Slightly better phasing of calculated and measured data was obtained for the first three rotor revolutions. The parameters for this match are also shown in figure 17.

One additional case was studied. This case differed from the previous one in that the simulation was forced with the same gyro angles as had been measured. The same parameters as for the seven-parameter case were allowed to vary; the precone angle, advance ratio, and the mechanical advantage constant were also allowed to vary from their nominal values. A total of 10 parameters could be adjusted by the identification program. Figure 18 shows the comparison for this case and the corresponding identified parameters are given in the figure. The gyro angles are in exact agreement in this case since the math model was forced with the measured gyro angles. The hub moment match is similar to that obtained in the previous case. The identification algorithm forced the magnitude of the hub moments to be the same, but better phasing of calculated and measured response over 10 rotor revolutions was not obtained. Limitations in the mathematical model or in the measured data used for the identification might have resulted in the lack of phase matching.

Discussion of Results

The parameters obtained from the identification program for the steady-state and transient cases studied are shown in tables 3 and 4. The tabulation of the parameters for each advance ratio shows a consistency in the magnitude of the estimated parameters. For the two steady-state cases investigated, the estimated values of 10 parameter cases were similar. For the transient run studied, some variation in the magnitude of the parameters was found when a large number of parameters were estimated. Some of the scatter in the estimated values of the 7 and 10 parameter cases may have been due to noise present in the measured data. Also, for both the steady-state and transient runs, the rotor was not lifting, which could make the contamination of the measured signal by noise more significant. Two other factors that may have influenced the lack of matching are deficiencies in the mathematical model and the range over which the parameters were allowed to vary in the

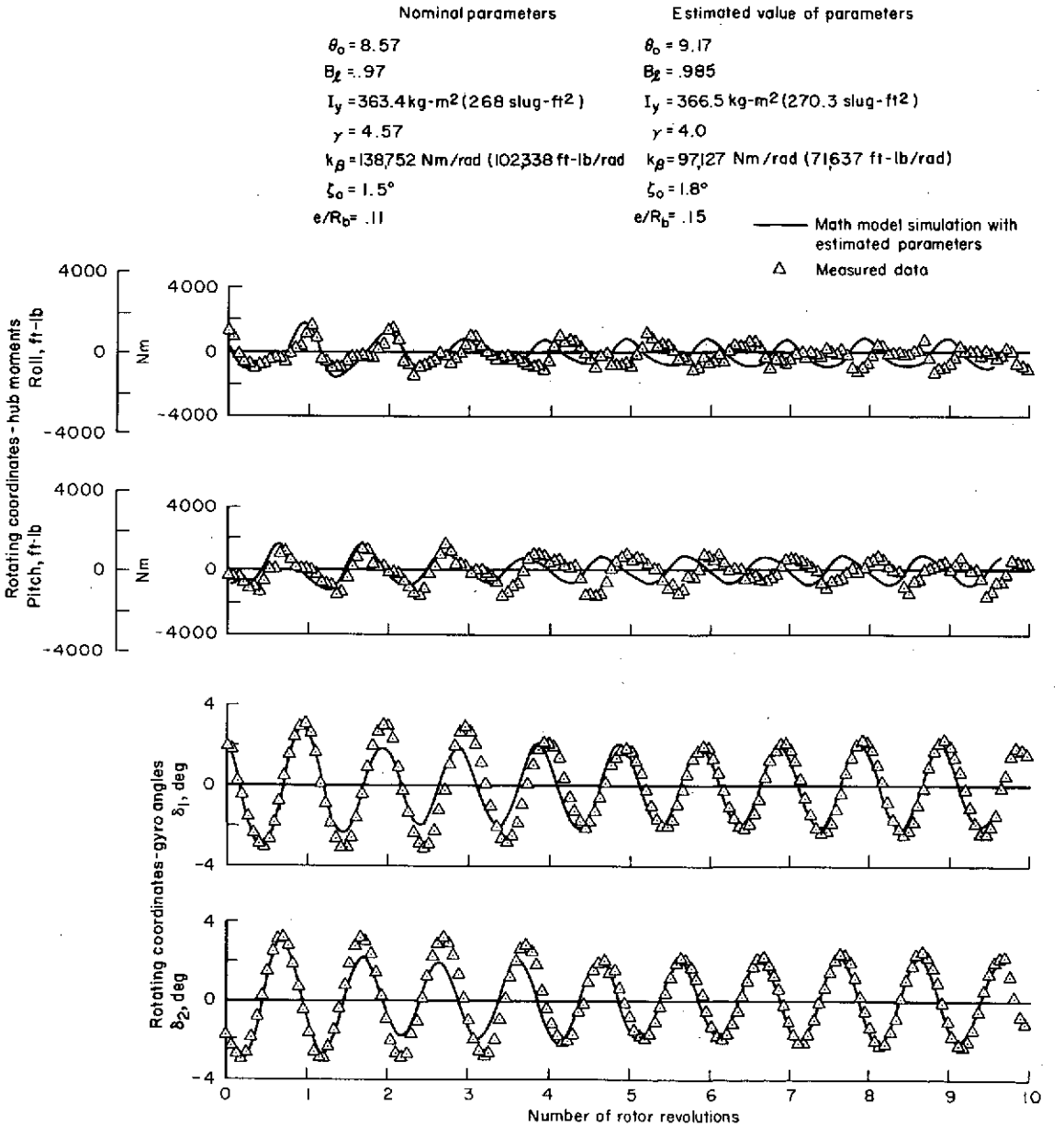

Figure 17.- Comparison of math model simulation with measured data using seven estimated parameters, μ = 0.355.

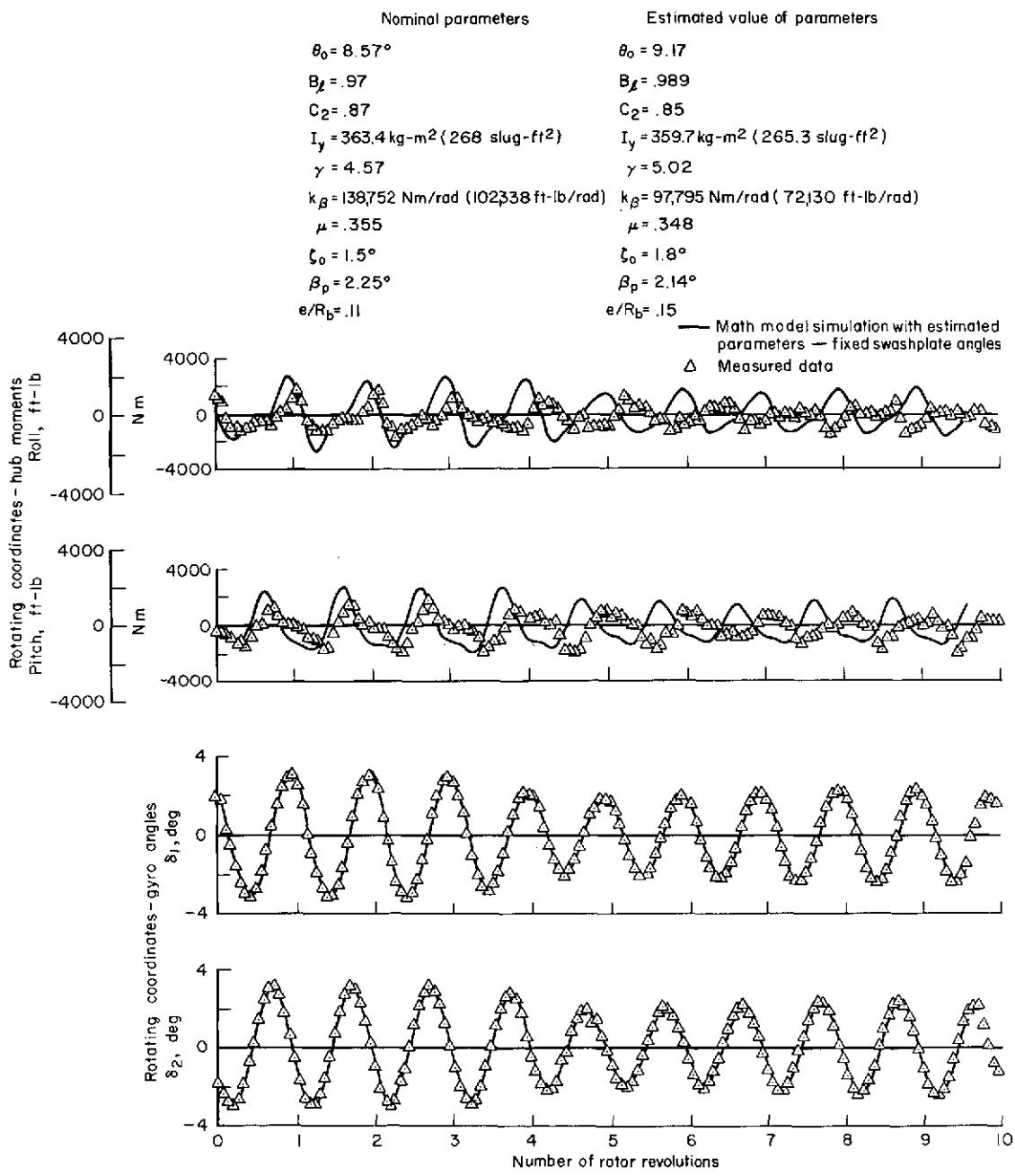

Figure 18.- Comparison of math model simulation with measured data using 10 parameters with fixed swashplate angles, μ = 0.355.

identification program. Only the flapping and feathering degrees of freedom were modeled here. But the inplane degree of freedom as well as blade torsional effects may be required in the mathematical model to obtain better matching of the measured data. The other factor influencing the time history matching is the limit imposed on the parameters over which the identification program could search. The limits on the parameters were set by the accuracies with which the parameters could be measured or estimated. An example is the spring constant of the blade, which is not constant for all rotor RPM and therefore is more difficult to determine. The virtual hinge location e is another parameter whose limits were not well defined. These factors will influence the time history matching obtained.

Note again that the identification in all cases was carried out over the first 2 or 3 rotor revolutions. But the comparisons of the simulated and measured data using the identified parameters are presented for 10 rotor revolutions. This was done to show that an improved match for a very short portion of the measured data resulted in an improved match throughout the entire transient range of the measured data. Convergence of the parameters to be estimated was usually obtained after five iterations. Larger numbers of iterations were performed and larger sets of parameters were estimated, but hub moment and gyro angle matching were not improved.

The identification program also calculates the sensitivity of the output to each parameter. The sensitivity was defined (ref. 9) as a dimensionless ratio of the change in the output due to a change in the parameter. For this model, the outputs are the roll and pitch hub moments and the roll and pitch gyro angles in rotating coordinates. A list of the sensitivities for the model parameters is given in table 5. Parameters of high sensitivity are collective angle (θ_o), twist angle (θ_1) of the blade, tip loss factor (B_ℓ), and blade to gyro coupling constant. The sensitivity of the next three parameters in order of decreasing sensitivity are Lock number (γ) (or blade inertia I_y, I_z), spring constant (k_β), and advance ratio (μ). Accurate measurements of collective angle, twist angle, and blade flapping inertia can be obtained as well as the Lock number (which can be analytically evaluated). But the values of spring constant as modeled here are difficult to evaluate since they are not constant for different flight conditions. The best method for obtaining improved estimates for some of these parameters is through the use of parameter identification techniques. The information gained from the sensitivity analysis portion of the identification technique used here can be very useful in determining where improvements in measurement or the analytical evaluation of parameters should be made.

It was found from the application of this identification technique that, to obtain refinements of the parameters for the mathematical model, two conditions must be satisfied. First, the mathematical model of the physical system must be complete except for constant parameters. Second, the values and the range of uncertainties for each of the unknown parameters should be specified either from analytical techniques or from measurements. Subject to these conditions, the identification technique is applicable to the estimation of parameters of complex rotor systems from wind-tunnel or flight data. Moreover, the utility of the method is evident in the identification of those

parameters that cannot be measured directly (such as the equivalent flapping hinge spring constant), but are computed indirectly by the algorithm through the complex relationship between the parameters and the measured response.

CONCLUSIONS

Comparisons of wind-tunnel data for advance ratios up to 0.40 with the mathematical model simulation indicate that the mathematical model derived here gives a reasonably good representation of the rotor hub moments in steady-state operation. The match between the mathematical model and the measured data was improved by adjusting selected model parameters with parameter identification techniques. As many as 10 parameters were estimated simultaneously.

For the transient runs with the rotor operating in a free gyro mode, considerably larger hub moments were calculated than measured. However, gyro angles during the transient operation were in close agreement with the math model simulation. An improved match in the magnitude of the hub moments could be achieved using parameter identification techniques, but phase matching of the time histories over a large number of rotor revolutions could not be obtained. More extensive mathematical modeling of the rotor is necessary to further improve the time history matching.

The sensitivity of the blade response to small changes in the parameters was calculated. The most sensitive parameters were collective pitch, blade twist, tip loss factor, blade to gyro coupling constant, Lock number, and equivalent flapping hinge spring constant.

Ames Research Center
National Aeronautics and Space Administration
Moffett Field, Calif., 94035, June 5, 1974

APPENDIX A

DERIVATION OF BLADE EQUATION

The rigid blade equations are derived in three parts: first, the moments due to inertial forces; second, the aerodynamic moments acting on the blade; and third, the mechanical moments that balance the inertial and aerodynamic moments on the blade. Figure 1 shows the gyro-controlled rotor to be modeled.

Inertia Moments

Figure 2 shows the right-handed coordinate system used to derive the equations for the blade. The X_s,Y_s,Z_s coordinates define the stationary coordinates of the blade. The X_s axis points rearward over the tail section of the helicopter while the Y_s axis points out of the right side of the hub. The Z_s axis points upward following the completion of the right-handed coordinate system. The coordinates X_r,Y_r,Z_r rotate at angular velocity Ω of the rotor whose reference point is taken from the stationary axis X_s. The positive directions of the flapping angle β, inplane ζ, and feathering angle θ are defined in figure 2.

In developing the inertia moments, the following definitions and assumptions were made:

(1) Only the first flapping mode is considered; it is represented by rigid blade motion about a spring-restrained virtual hinge located a distance e radially from the hub center.

(2) Blade feathering (pitch) is represented by rigid-body torsional motion.

(3) All deflection angles (β, θ, ζ) are small.

(4) The inplane degree of freedom is not represented.

The B frame (X_b,Y_b,Z_b) is defined by the rotations of β, ζ, and θ. The equations are developed in the B-frame since it represents the principal axes of the blade. The equations are then transferred to the R-frame (X_r, Y_r,Z_r), which is also referred to as the shaft axis system of the blade.

The rotational equations of motion in the B-frame (blade frame) are obtained by expanding the angular momentum equation for a rigid body (see ref. 10):

$$M_x = I_x\dot{\omega}_x + (I_z - I_y)\omega_y\omega_z \qquad \text{(A1}$$

$$M_y = I_y\dot{\omega}_y + (I_x - I_z)\omega_x\omega_z \qquad \text{(A2}$$

where the effect of hinge offset e will be added later. To further expand these equations, the angular velocities and angular rates must be expressed

in terms of the coordinates shown in figure 2. Since only the feathering and flapping equations are developed here, the angular velocities $\omega_x, \omega_y, \omega_z$ and the angular accelerations $\dot{\omega}_x$ and $\dot{\omega}_y$ are needed. In developing these terms, small-angle approximations are made and terms small compared to 1 are dropped, which gives (ref. 11)

$$\left.\begin{aligned} \omega_x &= \Omega\beta - \dot{\beta}\zeta + \dot{\theta} \\ \omega_y &= \Omega\theta - \Omega\zeta\beta - \dot{\beta} + \dot{\zeta}\theta \\ \omega_z &= \Omega + \dot{\beta}\theta + \dot{\zeta} \end{aligned}\right\} \tag{A3}$$

$$\left.\begin{aligned} \dot{\omega}_x &= \Omega\dot{\beta} - \ddot{\beta}\zeta + \ddot{\theta} - \dot{\beta}\dot{\zeta} \\ \dot{\omega}_y &= \Omega\dot{\theta} - \Omega\dot{\zeta}\beta - \Omega\zeta\dot{\beta} - \ddot{\beta} + \ddot{\zeta}\theta + \dot{\zeta}\dot{\theta} \end{aligned}\right\} \tag{A4}$$

Equations (A3) and (A4) are substituted into (A1) and (A2) and then expanded. In expanding these equations, some terms will cancel. Terms that involve products of three or more angles are dropped from the expansion since they represent higher-order effects that are not investigated here. The equations for the feathering and flapping moments are then

$$M_x = I_x(\ddot{\theta} + \Omega\dot{\beta} - \dot{\beta}\dot{\zeta} - \ddot{\beta}\zeta) + (I_z - I_y)[\Omega^2(\theta - \zeta\beta) + \Omega(-\dot{\beta} + 2\theta\dot{\zeta}) - \dot{\zeta}\dot{\beta}] \tag{A5}$$

$$M_y = I_y[-\ddot{\beta} + \Omega(\dot{\theta} - \dot{\zeta}\beta - \zeta\dot{\beta}) + \dot{\zeta}\dot{\theta} + \ddot{\zeta}\theta] + (I_x - I_z)[\Omega^2\beta + \Omega(\dot{\theta} + \dot{\zeta}\beta - \zeta\dot{\beta}) + \dot{\zeta}\dot{\theta}] \tag{A6}$$

which define the feathering and flapping moments in the blade frame. The inplane moment equation was not retained in this analysis, although the inplane degree of freedom is present in the M_x and M_y equations. This was done to model the forward sweep ζ_o of the blade. Since no inplane motion was allowed, the following substitution is made in equations (A5) and (A6): $\zeta = \zeta_o$, $\dot{\zeta} = 0$, $\ddot{\zeta} = 0$. Also, for later use, these equations are defined in terms of their reaction moments $M_{x_{inertia}}$ and $M_{y_{inertia}}$, which are given by the negative of the M_x and M_y equations. The equations in the B-frame that result from the above substitution are

$$M_{x_{inertia}} = -I_x(\ddot{\theta} + \Omega\dot{\beta} - \ddot{\beta}\zeta_o) - (I_z - I_y)[\Omega^2(\theta - \zeta_o\beta) - \Omega\dot{\beta}] \tag{A7}$$

$$M_{y_{inertia}} = I_y[\ddot{\beta} - \Omega(\dot{\theta} - \zeta_o\dot{\beta})] - (I_x - I_z)[\Omega^2\beta + \Omega(\dot{\theta} - \zeta_o\dot{\beta})] \tag{A8}$$

To the flapping equation (A8) must be added the term due to the effect of the hinge offset e. The contribution to the flapping equation of the

hinge offset is given by $(3/2)I_y[e/(R_b-e)]\Omega^2\beta$ (ref. 12) where e is the hinge offset and R_b, the blade radius. If the effect of the hinge offset is included in the flapping equation, the inertia moments in the B-frame are

$$M_{x_{inertia}} = -I_x\ddot{\theta}-(I_z-I_y)\Omega^2\theta+I_x\zeta_o\ddot{\beta}-(I_x+I_y-I_z)\Omega\dot{\beta}+(I_z-I_y)\zeta_o\Omega^2\beta \tag{A9}$$

$$M_{y_{inertia}} = I_y\ddot{\beta}+(I_x+I_y-I_z)\zeta_o\Omega\dot{\beta}-(I_x-I_z)\Omega^2\beta-(I_x+I_y-I_z)\Omega\dot{\theta}+\frac{3}{2}I_y\frac{e}{R_b-e}\Omega^2\beta \tag{A10}$$

The above equations will now be transformed to the R-frame (or shaft axis system) since the aerodynamic and mechanical moments are developed in this reference frame. The transformation between the B and R frames for small angles is given by

$$\begin{bmatrix}\bar{b}_1\\ \bar{b}_2\end{bmatrix} = \begin{bmatrix}1 & \zeta_o\\ -\zeta_o & 1\end{bmatrix}\begin{bmatrix}\bar{r}_1\\ \bar{r}_2\end{bmatrix} \tag{A11}$$

With the application of the transformation equation (A11), the inertia equations (A9) and (A10) can be expressed in the R-frame. In expanding the equations in the R-frame, the approximation $1+\zeta_o^2 \approx 1$, $I_x\zeta_o^2 << I_y$, and dropping the $I_x\zeta_o\ddot{\theta}$ term in the $M_{y_{inertia}}$ equation (because it was found to be small compared to the other terms) gives

$$M_{x_{inertia}} = -I_x\ddot{\theta}+(I_x+I_y-I_z)\zeta_o\Omega\dot{\theta}-(I_z-I_y)\Omega^2\theta+(I_x-I_y)\zeta_o\ddot{\beta}-(I_x+I_y-I_z)\Omega\dot{\beta}$$
$$+(I_x-I_y)\zeta_o\Omega^2\beta-\frac{3}{2}I_y\zeta_o\frac{e}{R_b-e}\Omega^2\beta \tag{A12}$$

$$M_{y_{inertia}} = I_y\ddot{\beta}-(I_x+I_y\zeta_o^2-I_z)\Omega^2\beta+\frac{3}{2}I_y\frac{e}{R_b-e}\Omega^2\beta-(I_x+I_y-I_z)\Omega\dot{\theta}-(I_z-I_y)\zeta_o\Omega^2\theta \tag{A13}$$

Equations (A12) and (A13) define the feathering and flapping moments of inertia in the R-frame.

Aerodynamic Moment

The aerodynamic moment is developed from the normal and tangential velocity components at the blade. The assumptions made in developing the aerodynamic moments are:

(1) The aerodynamic center of the blade is at the quarter chord.
(2) The inflow angle is small.
(3) Two inflow models were used - a uniform and a nonuniform model.

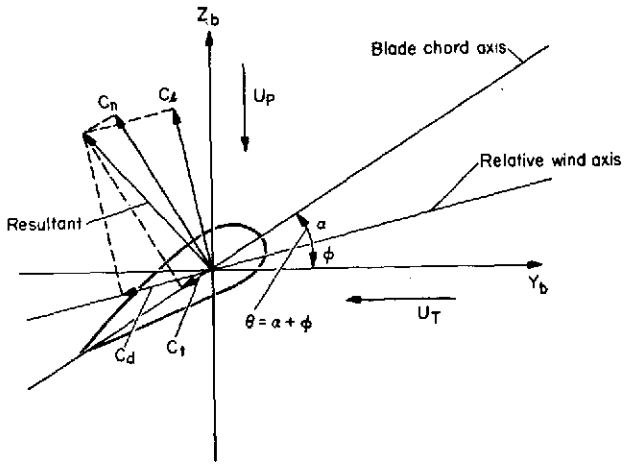

Sketch (a)

(4) The blade element lift coefficient curve is linear.

(5) The reverse flow region of the rotor was taken from 225° to 315° azimuth.

The coordinates used to develop the aerodynamic moments are shown in sketch (a). The aerodynamic moment about the flapping axis is given by

$$M_{y_{aero}} = -c \int_{e_\beta}^{B_\ell} c_n q r \, dr \qquad (A14)$$

In the reverse flow region, the limits of integration of equation (A14) were changed to account for the loss of lift in this region. The reverse flow region was taken from an azimuth angle of 225° to 315°. In this region, the lower limit in the aerodynamic moment equations was set equal to the advance ratio μ. Although the exact reverse flow region in forward flight is given by a circular disk of diameter μ (for the blade radius normalized by R_b), this approximation was used since it was more easily implemented for computational purposes. To expand equation (A14), expressions for the tangential velocity and perpendicular velocity components must be obtained. The dynamic pressure is given by

$$q = \rho \frac{U_T^2}{2} \left[1 + \left(\frac{U_P}{U_T} \right)^2 \right] \qquad (A15)$$

Since $(U_P/U_T)^2 << 1$, equation (A15) becomes

$$q = \rho (U_T^2/2) \qquad (A16)$$

From sketch (a), the angle of attack α of the blade is

$$\alpha = \theta - \phi \qquad (A17)$$

The inflow angle ϕ is

$$\phi = \tan^{-1}(U_P/U_T) \qquad (A18)$$

but, for small ϕ, a small-angle approximation is

$$\phi = U_P/U_T \qquad (A19)$$

For a symmetrical airfoil,

$$c_n \simeq c_\ell = a\alpha \qquad (A20)$$

Substituting for α in equation (A20) yields

$$c_n = a\left(\theta - \frac{U_P}{U_T}\right) \tag{A21}$$

The tangential and perpendicular velocity components required in equation (A21) are given by (ref. 11)

$$U_T = \Omega R_b\left[\frac{r}{R_b} + \frac{(r-e)}{\Omega R_b}\dot{\zeta} + \mu\zeta\cos\psi + \mu\sin\psi\right] \tag{A22}$$

$$U_P = \Omega R_b\left[\frac{(r-e)}{\Omega R_b}\dot{\beta} + \frac{r}{R_b}\zeta\beta + \mu\beta\cos\psi - \lambda\right] \tag{A23}$$

Neglecting the offset hinge aerodynamically and substituting $\zeta = \zeta_o$, $\dot{\zeta} = 0$ yields the tangential and perpendicular velocities:

$$U_T = \Omega R_b\left(\frac{r}{R_b} + \mu\zeta_o\cos\psi + \mu\sin\psi\right) \tag{A24}$$

$$U_P = \Omega R_b\left(\frac{r}{\Omega R_b}\dot{\beta} + \frac{r}{R_b}\zeta_o\beta + \mu\beta\cos\psi - \lambda\right) \tag{A25}$$

Now let

$$\left.\begin{aligned} x &= r/R_b \\ r &= R_b x \\ dr &= R_b\,dx \end{aligned}\right\} \tag{A26}$$

then

The aerodynamic moment about the flapping axis can now be obtained by expanding equation (A14). Substituting equations (A16) and (A21) into (A14) yields

$$M_{y_{aero}} = -\frac{c\rho a}{2}\int_e^{B_\ell R_b}(\theta U_T^2 - U_P U_T)r\,dr \tag{A27}$$

The pitch angle θ represents the sum of the following angles:

$$\theta = \theta(x) = \theta_o + \theta_{cyc} + x\theta_1 + \beta\tan\delta_3 \tag{A28}$$

where θ_o is the collective angle of the blade, θ_{cyc} is the cyclic pitch angle, θ_1 is the twist angle of the blade, and $\beta\tan\delta_3$ represents the contribution due to a δ_3 hinge. Equation (A27) can now be expanded by substituting equations (A24), (A25), (A26), and (A28):

$$M_{y_{aero}} = \frac{-c\rho a R_b^4 \Omega^2}{2} \int_{e/R_b}^{B_\ell} \left[(x+\mu\zeta_o \cos\psi+\mu \sin\psi)^2(\theta_o+\theta_{cyc}+x\theta_1+\beta \tan\delta_3) \right.$$

$$\left. -(x+\mu\zeta_o \cos\psi+\mu \sin\psi)\left(\frac{x}{\Omega}\dot{\beta}+x\zeta_o\beta+\mu\beta \cos\psi-\lambda_o-\lambda_x x \cos\psi-\lambda_y x \sin\psi\right)\right] x\, dx \tag{A29}$$

In the above equation, either a uniform or a nonuniform inflow model can be used. The inflow λ is expressed as

$$\lambda = \lambda_o + \lambda_x x \cos\psi + \lambda_y x \sin\psi \tag{A30}$$

where λ_o represents the average inflow and λ_x and λ_y represent a linear variation of inflow across the disk. The above equation for λ was used to integrate the aerodynamic moment equation ($M_{y_{aero}}$) along the blade span given by equation (A29). For the uniform inflow calculation, λ_x and λ_y were set to zero. The magnitude of λ_o for a given forward flight condition was then calculated from the following relationship (ref. 12):

$$\lambda_o \simeq \mu\alpha_s - \frac{(1/2)C_t}{\mu(\mu^2 + \lambda_o^2)^{1/2}} \tag{A31}$$

For the nonuniform inflow calculation, λ_o, λ_x, and λ_y were estimated from measured wind-tunnel data for a particular flight condition. Equation (A29) is integrated from the hinge offset location to the tip of the blade (or tip loss factor since the equation has been normalized by $x = r/R$), and making use of the definition of the Lock number

$$\gamma = \frac{c\rho a R_b^4}{I_y} \tag{A32}$$

gives, for the aerodynamic moment about the flapping axis,

$$M_{y_{aero}} = -\frac{\gamma I_y \Omega^2}{2}\left\{-\left[\frac{1}{\Omega}\left(\frac{B_\ell^4}{4}-\frac{e^4}{4R_b^4}\right)+\frac{\mu}{\Omega}(\zeta_o\cos\psi+\sin\psi)\left(\frac{B_\ell^3}{3}-\frac{e^3}{3R_b^3}\right)\right]\dot{\beta}\right.$$

$$-\left[\zeta_o\left(\frac{B_\ell^4}{4}-\frac{e^4}{4R_b^4}\right)+\mu(\cos\psi+\zeta_o\sin\psi)\left(\frac{B_\ell^3}{3}-\frac{e^3}{3R_b^3}\right)+\frac{1}{2}\mu^2(\zeta_o+\zeta_o\cos 2\psi+\sin 2\psi)\right.$$

$$\times\left.\left(\frac{B_\ell^2}{2}-\frac{e^2}{2R_b^2}\right)\right]\beta+\left[\left(\frac{B_\ell^4}{4}-\frac{e^4}{4R_b^4}\right)+2\mu(\zeta_o\cos\psi+\sin\psi)\left(\frac{B_\ell^3}{3}-\frac{e^3}{3R_b^3}\right)\right.$$

$$\left.+\mu^2\left(\frac{1}{2}-\frac{1}{2}\cos 2\psi+\zeta_o\sin 2\psi\right)\left(\frac{B_\ell^2}{2}-\frac{e^2}{2R_b^2}\right)\right]\beta\tan\delta_3+\left[\left(\frac{B_\ell^5}{5}-\frac{e^5}{5R_b^5}\right)\right.$$

$$\left.+2\mu(\zeta_o\cos\psi+\sin\psi)\left(\frac{B_\ell^4}{4}-\frac{e^4}{4R_b^4}\right)+\mu^2\left(\frac{1}{2}-\frac{1}{2}\cos 2\psi+\zeta_o\sin 2\psi\right)\left(\frac{B_\ell^3}{3}-\frac{e^3}{3R_b^3}\right)\right]\theta_1$$

$$+\left[\left(\frac{B_\ell^4}{4}-\frac{e^4}{4R_b^4}\right)+2\mu(\zeta_o\cos\psi+\sin\psi)\left(\frac{B_\ell^3}{3}-\frac{e^3}{3R_b^3}\right)+\mu^2\left(\frac{1}{2}-\frac{1}{2}\cos 2\psi+\zeta_o\sin 2\psi\right)\right.$$

$$\times\left.\left(\frac{B_\ell^2}{2}-\frac{e^2}{2R_b^2}\right)\right](\theta_o+\theta_{cyc})+\left[\left(\frac{B_\ell^3}{3}-\frac{e^3}{3R_b^3}\right)+\mu(\zeta_o\cos\psi+\sin\psi)\left(\frac{B_\ell^2}{2}-\frac{e^2}{2R_b^2}\right)\right]\lambda_o$$

$$+\left[\left(\frac{B_\ell^4}{4}-\frac{e^4}{4R_b^4}\right)\cos\psi+\mu(\cos\psi\sin\psi+\zeta_o\cos^2\psi)\left(\frac{B_\ell^3}{3}-\frac{e^3}{3R_b^3}\right)\right]\lambda_x$$

$$+\left.\left[\left(\frac{B_\ell^4}{4}-\frac{e^4}{4R_b^4}\right)\sin\psi+\mu(\sin^2\psi+\zeta_o\cos\psi\sin\psi)\left(\frac{B_\ell^3}{3}-\frac{e^3}{3R_b^3}\right)\right]\lambda_y\right\} \qquad \text{(A33)}$$

To simplify this equation in the main body of the text, the following definitions are made:

$$\left.\begin{aligned} K1 &= \frac{\gamma I_y \Omega^2}{2}, \quad B2 = \frac{B^2}{2}-\frac{e^2}{2R_b^2}, \quad B3 = \frac{B^3}{3}-\frac{e^3}{3R_b^3} \\ B4 &= \frac{B^4}{4}-\frac{e^4}{4R_b^4}, \quad B5 = \frac{B^5}{5}-\frac{e^5}{5R_b^5} \end{aligned}\right\} \qquad \text{(A34)}$$

$$
\left.
\begin{aligned}
C1(\psi) &= \zeta_o B4 + \mu(\cos\psi + \zeta_o \sin\psi)B3 + \tfrac{1}{2}\mu^2(\zeta_o + \zeta_o \cos 2\psi + \sin 2\psi)B2 \\
C2(\psi) &= \frac{B4}{\Omega} + \frac{\mu}{\Omega}(\zeta_o \cos\psi + \sin\psi)B3 \\
C3(\psi) &= B5 + 2\mu(\zeta_o \cos\psi + \sin\psi)B4 + \mu^2\left(\tfrac{1}{2} - \tfrac{1}{2}\cos 2\psi + \zeta_o \sin 2\psi\right)B3 \\
C4(\psi) &= B4 + 2\mu(\zeta_o \cos\psi + \sin\psi)B3 + \mu^2\left(\tfrac{1}{2} - \tfrac{1}{2}\cos 2\psi + \zeta_o \sin 2\psi\right)B2 \\
C5(\psi) &= B3 + \mu(\zeta_o \cos\psi + \sin\psi)B2 \\
C6(\psi) &= B4 \cos\psi + \mu(\cos\psi \sin\psi + \zeta_o \cos^2\psi)B3 \\
C7(\psi) &= B4 \sin\psi + \mu(\sin^2\psi + \zeta_o \cos\psi \sin\psi)B3
\end{aligned}
\right\} \quad (A35)
$$

The aerodynamic moment about the flapping axis can now be written in a more compact form by use of equations (A34) and (A35):

$$
\begin{aligned}
M_{y_{aero}} = -K1\{&-C2(\psi)\dot{\beta} + [-C1(\psi) + C4(\psi)\tan\delta_3]\beta + C3(\psi)\theta_1 + C4(\psi)\theta_o \\
&+C4(\psi)\theta_{cyc} + C5(\psi)\lambda_o + C6(\psi)\lambda_x + C7(\psi)\lambda_y\}
\end{aligned} \quad (A36)
$$

For the reverse flow region, the lower limit of equation (A29) is equal to μ, which results in a change of the e/R_b terms in equation (A34) to the advance ratio μ. In the simulation of equation (A36), the appropriate coefficients were substituted when the retreating blade was in the reverse flow region.

The aerodynamic moment about the flapping axis is given by equation (A36). The aerodynamic moment about the feathering axis was found to be very small and therefore was not included in the analysis.

Mechanical Moments

The inertia moment about the feathering axis of the blade is balanced by gyro moments and the flapping moments that couple into the feathering axis due to the forward sweep (ζ_o) of the blade. In addition, spring and damping moments about the feathering axis must be included. This moment balance is established in appendix B where the complete gyro equations are developed. For the flapping degree of freedom, the inertial and aerodynamic moments are balanced by the spring restraint of the blade with spring constant k_β. The mechanical moments about the flapping axis can then be written as

$$M_{y_{mech}} = k_\beta(\beta - \beta_p) \tag{A37}$$

where β and β_p are the flapping and precone angles of the blade. The sum of the inertia, aerodynamic, and mechanical moments about the flapping axis must sum to zero to obtain a moment balance. The resulting equation for the flapping axis is then

$$I_y\ddot{\beta}-(I_x+I_y\zeta_o^2-I_z)\Omega^2\beta+\frac{3}{2}I_y\frac{e}{R_b-e}\Omega^2\beta-(I_x+I_y-I_z)\Omega\dot{\theta}-(I_z-I_y)\zeta_o\Omega^2\theta-K1\{-C2(\psi)\dot{\beta}$$

$$+[-C1(\psi)+C4(\psi)\tan\delta_3]\beta+C3(\psi)\theta_1+C4(\psi)\theta_o+C4(\psi)\theta_{cyc}+C5(\psi)\lambda_o+C6(\psi)\lambda_x+C7(\psi)\lambda_y\}$$

$$+k_\beta(\beta-\beta_p) = 0 \tag{A38}$$

This completes the development of the blade equations. The abbreviated notation for the aerodynamic terms in equation (A38) was used to simplify the equation in the main body of the text. In the remainder of this appendix, the flapping equation is developed for any number of blades from which the equations for the particular three-bladed rotor are obtained. The flapping equation (A38) can be written in general terms for any number of blades as

$$I_y\ddot{\beta}_i-(I_x+I_y\zeta_o^2-I_z)\Omega^2\beta_i+\frac{3}{2}I_y\frac{e}{R-e}\Omega^2\beta_i-(I_x+I_y-I_z)\Omega\dot{\theta}_i-(I_z-I_y)\zeta_o\Omega^2\theta_i$$

$$-K1\Bigg\{-C2\left[\psi+(i-1)\frac{2\pi}{b}\right]\dot{\beta}_i-C1\left[\psi+(i-1)\frac{2\pi}{b}\right]\beta_i+C4\left[\psi+(i-1)\frac{2\pi}{b}\right]\beta_i\tan\delta_3$$

$$+C3\left[\psi+(i-1)\frac{2\pi}{b}\right]\theta_1+C4\left[\psi+(i-1)\frac{2\pi}{b}\right](\theta_o+\theta_{cyc})+C5\left[\psi+(i-1)\frac{2\pi}{b}\right]\lambda_o$$

$$+C6\left[\psi+(i-1)\frac{2\pi}{b}\right]\lambda_x+C7\left[\psi+(i-1)\frac{2\pi}{b}\right]\lambda_y\Bigg\}+k_\beta(\beta_i-\beta_p) = 0\ ; \quad i = 1,2,\ldots,b \tag{A39}$$

where b is the number of blades. The feathering angles in equation (A39) are expressed in terms of gyro coordinates δ_1 and δ_2. The feathering angle θ_i is transformed to gyro coordinates δ_1 and δ_2 by

$$\theta_i = C_2\left[\delta_1\cos(i-1)\frac{2\pi}{b}+\delta_2\sin(i-1)\frac{2\pi}{b}\right]\ ; \quad i = 1,\ldots,b \tag{A40}$$

The derivatives of the feathering angles are obtained from equation (A40) by differentiation. Equation (A39) can now be expressed for a three-bladed rotor by varying the index $i = 1, 2, \ldots, b$ where $b = 3$, and by transforming the feathering angles and their derivatives with equation (A40). The complete flapping equations for the three-bladed rotor expressed in terms of the flapping angles and gyro angles are given by

$$I_y\ddot{\beta}_1-(I_x+I_y\zeta_o^2-I_z)\Omega^2\beta_1+\frac{3}{2}I_y\frac{e}{R-e}\Omega^2\beta_1-(I_x+I_y-I_z)\Omega C_2\dot{\delta}_1-(I_z-I_y)\zeta_o\Omega^2C_2\delta_1$$

$$-\frac{\gamma I_y\Omega^2}{2}\left\{-\left[\frac{B4}{\Omega}+\frac{\mu}{\Omega}(\zeta_o\cos\psi+\sin\psi)B3\right]\dot{\beta}-\left[\zeta_oB4+\mu(\cos\psi+\zeta_o\sin\psi)B3\right.\right.$$

$$+\frac{1}{2}\mu^2(\zeta_o+\zeta_o\cos 2\psi+\sin 2\psi)B2\Big]\beta_1+\Big[B4+2\mu(\zeta_o\cos\psi+\sin\psi)B3+\mu^2\Big(\frac{1}{2}-\frac{1}{2}\cos 2\psi$$

$$+\zeta_o\sin 2\psi\Big)B2\Big]\beta_1\tan\delta_3+\Big[B5+2\mu(\zeta_o\cos\psi+\sin\psi)B4+\mu^2\Big(\frac{1}{2}-\frac{1}{2}\cos 2\psi+\zeta_o\sin 2\psi\Big)B3\Big]\theta_1$$

$$+\Big[B4+2\mu(\zeta_o\cos\psi+\sin\psi)B3+\mu^2\Big(\frac{1}{2}-\frac{1}{2}\cos 2\psi+\zeta_o\sin 2\psi\Big)B2\Big](\theta_o+\theta_{cyc})$$

$$+[B3+\mu(\zeta_o\cos\psi+\sin\psi)B2]\lambda_o+[B4\cos\psi+\mu(\cos\psi\sin\psi+\zeta_o\cos^2\psi)B3]\lambda_x$$

$$\left.+[B4\sin\psi+\mu(\sin^2\psi+\zeta_o\cos\psi\sin\psi)B3]\lambda_y\right\}+k_\beta(\beta_1-\beta_p)=0 \qquad (A41)$$

$$I_y\ddot{\beta}_2-(I_x+I_y\zeta_o^2-I_z)\Omega^2\beta_2+\frac{3}{2}I_y\frac{e}{R-e}\Omega^2\beta_2-(I_x+I_y-I_z)\Omega C_2\Big(-\frac{1}{2}\dot{\delta}_1+\frac{\sqrt{3}}{2}\dot{\delta}_2\Big)$$

$$-(I_z-I_y)\zeta_o\Omega^2C_2\Big(-\frac{1}{2}\delta_1+\frac{\sqrt{3}}{2}\delta_2\Big)-\frac{\gamma I_y\Omega^2}{2}\left(-\left\{\frac{B4}{\Omega}+\frac{\mu}{\Omega}[\zeta_o\cos(\psi+120^\circ)+\sin(\psi+120^\circ)]B3\right\}\right.$$

$$\times\dot{\beta}_2-\Big\{\zeta_oB4+\mu[\cos(\psi+120^\circ)+\zeta_o\sin(\psi+120^\circ)]B3+\frac{1}{2}\mu^2[\zeta_o+\zeta_o\cos 2(\psi+120^\circ)$$

$$+\sin 2(\psi+120^\circ)]B2\Big\}\beta_2+\Big\{B4+2\mu[\zeta_o\cos(\psi+120^\circ)+\sin(\psi+120^\circ)]B3$$

$$+\mu^2\Big[\frac{1}{2}-\frac{1}{2}\cos 2(\psi+120^\circ)+\zeta_o\sin 2(\psi+120^\circ)\Big]B2\Big\}\beta_2\tan\delta_3+\Big\{B5+2\mu[\zeta_o\cos(\psi+120^\circ)$$

$$+\sin(\psi+120^\circ)]B4+\mu^2\Big[\frac{1}{2}-\frac{1}{2}\cos 2(\psi+120^\circ)+\zeta_o\sin 2(\psi+120^\circ)\Big]B3\Big\}\theta_1$$

$$+\Big\{B4+2\mu[\zeta_o\cos(\psi+120^\circ)+\sin(\psi+120^\circ)]B3+\mu^2\Big[\frac{1}{2}-\frac{1}{2}\cos 2(\psi+120^\circ)+\zeta_o\sin 2(\psi+120^\circ)\Big]$$

$$\times B2\Big\}(\theta_o+\theta_{cyc})+\{B3+\mu[\zeta_o\cos(\psi+120^\circ)+\sin(\psi+120^\circ)]B2\}\lambda_o+\{B4\cos(\psi+120^\circ)$$

$$+\mu[\cos(\psi+120^\circ)\sin(\psi+120^\circ)+\zeta_o\cos^2(\psi+120^\circ)]B3\}\lambda_x+\{B4\sin(\psi+120^\circ)+\mu[\sin^2(\psi+120^\circ)$$

$$\left.+\zeta_o\cos(\psi+120^\circ)\sin(\psi+120^\circ)]B3\}\lambda_y\right)+k_\beta(\beta_2-\beta_p)=0 \qquad (A42)$$

$$I_y\ddot{\beta}_3-(I_x+I_y\zeta_o^2-I_z)\Omega^2\beta_3+\frac{3}{2}I_y\frac{e}{R-e}\Omega^2\beta_3-(I_x+I_y-I_z)\Omega C_2\left(-\frac{1}{2}\dot{\delta}_1-\frac{\sqrt{3}}{2}\dot{\delta}_2\right)$$

$$-(I_z-I_y)\zeta_o\Omega^2C_2\left(-\frac{1}{2}\delta_1-\frac{\sqrt{3}}{2}\delta_2\right)-\frac{\gamma I_y\Omega^2}{2}\left(-\left\{\frac{B4}{\Omega}+\frac{\mu}{\Omega}[\zeta_o\cos(\psi+240°)+\sin(\psi+240°)]B3\right\}\right.$$

$$\times\dot{\beta}_3-\left\{\zeta_oB4+\mu[\cos(\psi+240°)+\zeta_o\sin(\psi+240°)]B3+\frac{1}{2}\mu^2[\zeta_o+\zeta_o\cos 2(\psi+240°)\right.$$

$$\left.+\sin 2(\psi+240°)]B2\right\}\beta_3+\left\{B4+2\mu[\zeta_o\cos(\psi+240°)+\sin(\psi+240°)]B3\right.$$

$$\left.+\mu^2\left[\frac{1}{2}-\frac{1}{2}\cos 2(\psi+240°)+\zeta_o\sin 2(\psi+240°)\right]B2\right\}\beta_3\tan\delta_3+\left\{B5+2\mu[\zeta_o\cos(\psi+240°)\right.$$

$$\left.+\sin(\psi+240°)]B4+\mu^2\left[\frac{1}{2}-\frac{1}{2}\cos 2(\psi+240°)+\zeta_o\sin 2(\psi+240°)\right]B3\right\}\theta_1$$

$$+\left\{B4+2\mu[\zeta_o\cos(\psi+240°)+\sin(\psi+240°)]B3+\mu^2\left[\frac{1}{2}-\frac{1}{2}\cos 2(\psi+240°)+\zeta_o\sin 2(\psi+240°)\right]\right.$$

$$\left.\times B2\right\}(\theta_o+\theta_{cyc})+\{B3+\mu[\zeta_o\cos(\psi+240°)+\sin(\psi+240°)]B2\}\lambda_o+\{B4\cos(\psi+240°)$$

$$+\mu[\cos(\psi+240°)\sin(\psi+240°)+\zeta_o\cos^2(\psi+240°)]B3\}\lambda_x+B4\{\sin(\psi+240°)+\mu[\sin^2(\psi+240°)$$

$$\left.+\zeta_o\cos(\psi+240°)\sin(\psi+240°)]B3\}\lambda_y\right)+k_\beta(\beta_3-\beta_p)=0 \qquad \text{(A43)}$$

APPENDIX B

DERIVATION OF GYRO EQUATION

The gyro of the rotor modeled was located at the top of the rotor head and was operated at about 10,000 RPM. The gyro and the rotor head are shown in sketch (b). This sketch is shown here only for mathematical modeling purposes and does not necessarily represent the exact mechanical connection of the gyro with the rotor. The X_S, Y_S, Z_S coordinates represent the stationary coordinates of the rotor. Since the body motion of the helicopter was not modeled, the X_S, Y_S, Z_S coordinates also serve as the inertial coordinates for the development of the gyro equations. The X_r, Y_r, Z_r coordinates are the rotating coordinates or the shaft axes of the blade while the X_c, Y_c, Z_c coordinates are the coordinates of the gyro at an angle ψ_o from the X_r, Y_r, Z_r frame. One more coordinate system must be defined for the gyro itself since it rotates at a much higher speed than the rotor. This coordinate system is defined by the X_g, Y_g, Z_g axes system. With the definition of these coordinates, the gyro equations and the equations for the gyro-blade interaction are derived.

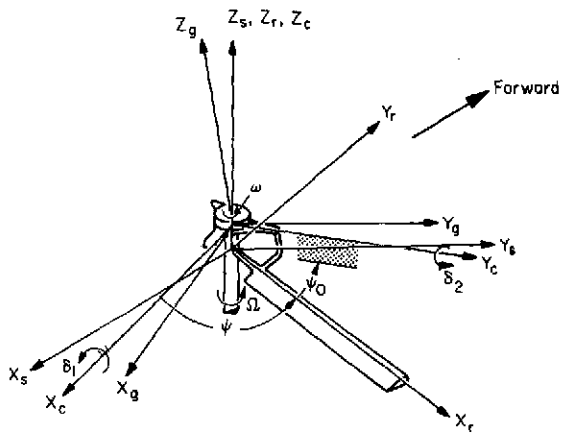

Sketch (b)

The rate of change of angular momentum of the gyro is given by Newton's second law:

$$\left[\frac{d\bar{H}_G}{dt}\right]_S = \bar{M}_G \tag{B1}$$

where the angular momentum of the gyro is

$$\bar{H}_G = \bar{\bar{I}} \cdot \bar{\omega}_{G/S} \tag{B2}$$

Since no body motion was allowed (as mentioned in the definition of the coordinates), the stationary frame X_S, Y_S, Z_S serves as the inertial frame in the development of the gyro equations.

The rate of change of angular momentum of the gyro with respect to the C frame is expressed as

$$\bar{\bar{I}}_G \cdot \left[\frac{d\bar{\omega}_{G/S}}{dt}\right]_C + \bar{\omega}_{C/S} \times \bar{\bar{I}}_G \cdot \bar{\omega}_{G/S} = \bar{M}_G \tag{B3}$$

To expand equation (B3), the angular velocities between reference frames must be established. The angular velocity of the gyro with respect to inertial space is

$$\bar{\omega}_{G/S} = \bar{\omega}_{G/C} + \bar{\omega}_{C/R} + \bar{\omega}_{R/S} \tag{B4}$$

The angular velocity of the C frame with respect to inertial space is

$$\bar{\omega}_{C/S} = \bar{\omega}_{C/R} + \bar{\omega}_{R/S} \tag{B5}$$

The angular velocities in equations (B4) and (B5) are

$$\bar{\omega}_{G/C} = [\bar{c}_1, \bar{c}_2, \bar{c}_3] \begin{bmatrix} 0 \\ 0 \\ \omega \end{bmatrix} \tag{B6}$$

$$\bar{\omega}_{C/R} = [\bar{g}_1, \bar{g}_2, \bar{g}_3] \begin{bmatrix} \dot{\delta}_1 \\ \dot{\delta}_2 \\ 0 \end{bmatrix} \tag{B7}$$

$$\bar{\omega}_{R/S} = [\bar{g}_1, \bar{g}_2, \bar{g}_3] \begin{bmatrix} 0 \\ 0 \\ \Omega \end{bmatrix} \tag{B8}$$

The transformation between the C and G frame, considering only small angles, is

$$\begin{bmatrix} \bar{c}_1 \\ \bar{c}_2 \\ \bar{c}_3 \end{bmatrix} = \begin{bmatrix} 1 & 0 & -\delta_2 \\ 0 & 1 & \delta_1 \\ \delta_2 & -\delta_1 & 1 \end{bmatrix} \begin{bmatrix} \bar{g}_1 \\ \bar{g}_2 \\ \bar{g}_3 \end{bmatrix} \tag{B9}$$

Equation (B4) can be expressed in the C frame by use of equations (B6), (B7), and (B8) and the transformation equation (B9):

$$\bar{\omega}_{G/S} = [\bar{c}_1, \bar{c}_2, \bar{c}_3] \begin{bmatrix} \dot{\delta}_1 - \Omega\delta_2 \\ \dot{\delta}_2 + \Omega\delta_1 \\ \omega_G \end{bmatrix} \tag{B10}$$

where $\omega_G = \omega + \Omega$ and terms such as $\dot{\delta}_1\delta_2$ and $\delta_1\dot{\delta}_2$ are considered negligible. The angular rate $\dot{\bar{\omega}}_{G/S}$ can be obtained from equation (B10) by differentiation:

$$\dot{\bar{\omega}}_{G/S} = [\bar{c}_1, \bar{c}_2, \bar{c}_3] \begin{bmatrix} \ddot{\delta}_1 - \Omega\dot{\delta}_2 \\ \ddot{\delta}_2 + \Omega\dot{\delta}_1 \\ 0 \end{bmatrix} \tag{B11}$$

Equation (B5) can also be expressed in the C frame by use of equations (B7) and (B8) and transformation equation (B9):

$$\bar{\omega}_{C/S} = [\bar{c}_1, \bar{c}_2, \bar{c}_3] \begin{bmatrix} \dot{\delta}_1 - \Omega\delta_2 \\ \dot{\delta}_2 + \Omega\delta_1 \\ \Omega \end{bmatrix} \tag{B12}$$

Since the gyro is modeled as a disk, the diametrical inertias are equal, defined as $I_G = I_1 = I_2$. The inertia through the center of rotation of the disk is I_3. The inertia distribution of the gyro is then

$$\bar{\bar{I}}_G = [\bar{c}_1, \bar{c}_2, \bar{c}_3] \begin{bmatrix} I_G & 0 & 0 \\ 0 & I_G & 0 \\ 0 & 0 & I_3 \end{bmatrix} \begin{bmatrix} \bar{c}_1 \\ \bar{c}_2 \\ \bar{c}_3 \end{bmatrix} \tag{B13}$$

Substituting the above equations for the angular velocities, rates, and inertia distribution into equation (B3) gives the following equations for the gyro:

$$I_G\ddot{\delta}_1 + (I_3\Omega\omega_G - I_G\Omega^2)\delta_1 + (I_3\omega_G - 2\Omega I_G)\dot{\delta}_2 = M_{G_x} \tag{B14}$$

$$I_G\ddot{\delta}_2 + (I_3\Omega\omega_G - I_G\Omega^2)\delta_2 - (I_3\omega_G - 2\Omega I_G)\dot{\delta}_1 = M_{G_y} \tag{B15}$$

For a high-speed gyro, ω_G will be some multiple value of the rotor speed Ω. Hence let

$$\omega_G = k_R\Omega \tag{B16}$$

where k_R is some multiple of the rotor speed. Substituting equation (B16) into (B14) and (B15) gives for the gyro equations:

$$I_G\ddot{\delta}_1 + (I_3\Omega^2 k_R - I_G\Omega^2)\delta_1 + (I_3 k_R\Omega - 2\Omega I_G)\dot{\delta}_2 = M_{G_x} \tag{B17}$$

$$I_G\ddot{\delta}_2 + (I_3\Omega^2 k_R - I_G\Omega^2)\delta_2 - (I_3 k_R\Omega - 2\Omega I_G)\dot{\delta}_1 = M_{G_y} \tag{B18}$$

In the following section, the external moments M_{G_x} and M_{G_y} of equations (B17) and (B18) are developed.

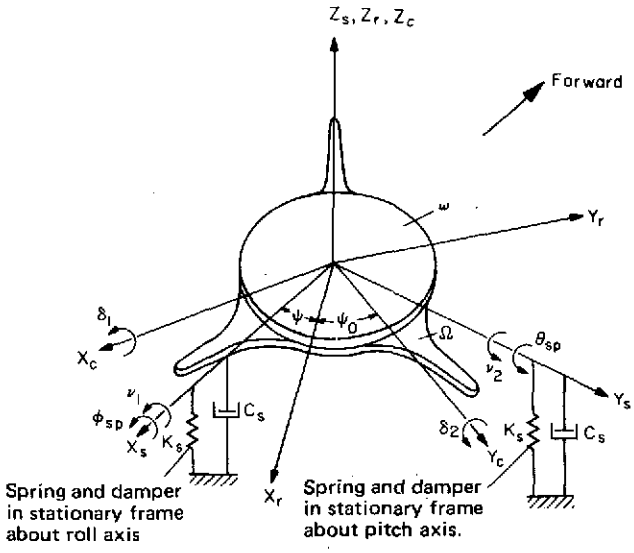

Sketch (c)

First, the pilot's swashplate roll and pitch moment inputs (ν_1 and ν_2) and the swashplate damping and spring terms are developed and, second, the excitation of the gyro by the blade is derived. The sum of the above moments in rotating gyro coordinates constitutes the external moments M_{G_x} and M_{G_y}. A sketch of the gyro disk with the springs, dampers, and moments inputs is presented in sketch (c). These moments were measured in the stationary axis system (X_s, Y_s, Z_s) and must be transferred to the rotating gyro axis system (X_c, Y_c, Z_c).

The moments in the stationary axis system due to pilot input and the spring and damper are

$$M_{x_s} = \nu_1 - C_s \dot{\phi}_{sp} - K_s \phi_{sp} \tag{B19}$$

$$M_{y_s} = \nu_2 - C_s \dot{\theta}_{sp} - K_s \theta_{sp} \tag{B20}$$

The above equations must now be transformed to rotating coordinates since all equations in this development are expressed in the rotating coordinate system. The transformation between the stationary and the rotating coordinates is given by

$$\begin{bmatrix} \bar{s}_1 \\ \bar{s}_2 \end{bmatrix} = \begin{bmatrix} \sin(\psi+\psi_o) & \cos(\psi+\psi_o) \\ -\cos(\psi+\psi_o) & \sin(\psi+\psi_o) \end{bmatrix} \begin{bmatrix} \bar{c}_1 \\ \bar{c}_2 \end{bmatrix} \tag{B21}$$

or, between gyro angles and swashplate angles, by

$$\begin{bmatrix} \phi_{sp} \\ \phi_{sp} \end{bmatrix} = \begin{bmatrix} \sin(\psi+\psi_o) & \cos(\psi+\psi_o) \\ -\cos(\psi+\psi_o) & \sin(\psi+\psi_o) \end{bmatrix} \begin{bmatrix} \delta_1 \\ \delta_2 \end{bmatrix} \tag{B22}$$

Equations (B19) and (B20) can be transformed to rotating coordinates by applying transformations (B21) and (B22). In addition to the pilot input and the spring and damper moments, the excitation of the gyro by the blade $M_{exc_{xc}}$ and $M_{exc_{yc}}$ must be added to give the complete set of applied external moments for equations (B17) and (B18):

$$M_{G_x} = \nu_1 \sin(\psi + \psi_o) - \nu_2 \cos(\psi + \psi_o) + \Omega C_s \delta_2 - C_s \dot{\delta}_1 - K_s \delta_1 + M_{exc_{xc}} \tag{B23}$$

$$M_{G_y} = \nu_1 \cos(\psi + \psi_o) + \nu_2 \sin(\psi + \psi_o) - \Omega C_s \delta_1 - C_s \dot{\delta}_2 - K_s \delta_2 + M_{exc_{yc}} \tag{B24}$$

The gyro equations can be written from equations (B17), (B18), (B23), and (B24) as

$$I_G \ddot{\delta}_1 + (I_3 \Omega^2 k_R - I_G \Omega^2)\delta_1 + (I_3 \Omega k_R - 2\Omega I_G)\dot{\delta}_2 - \Omega C_s \delta_2 + C_s \dot{\delta}_1 + K_s \delta_1 - M_{exc_{xc}} = \nu_1 \sin(\psi + \psi_o) - \nu_2 \cos(\psi + \psi_o) \tag{B25}$$

$$I_G \ddot{\delta}_2 + (I_3 \Omega^2 k_R - I_G \Omega^2)\delta_2 - (I_3 \Omega k_R - 2\Omega I_G)\dot{\delta}_1 + \Omega C_s \delta_1 + C_s \dot{\delta}_2 + K_s \delta_2 - M_{exc_{yc}} = \nu_1 \cos(\psi + \psi_o) + \nu_2 \sin(\psi + \psi_o) \tag{B26}$$

The only remaining terms to be expanded is the excitation of the gyro by blade $M_{exc_{xc}}$ and $M_{exc_{yc}}$. These are the moments in gyro rotating coordinates (X_c, Y_c) which are transmitted through mechanical linkages from the feathering axis of the blade. The moment about the feathering axis for one blade in the rotating blade coordinate (X_r, Y_r, Z_r) system is given by (ref. 13)

$$M_{exc} = \zeta_o M_{y_{mech}} + \zeta_o M_{y_{inertia}} + M_{x_{inertia}} - k_\theta \theta - c_\theta \dot{\theta} \tag{B27}$$

The moments $M_{y_{mech}}$ and $M_{y_{inertia}}$ are the mechanical and inertia moments that couple into the feathering axis because of the forward sweep ζ_o of the blade. The inertia moment about the feathering axis is given by $M_{x_{inertia}}$. The $k_\theta \theta$ and $c_\theta \dot{\theta}$ terms represent the spring and damping effects about the feathering axis. Equation (B27) is expanded by substituting for the inertia and mechanical moments from equations (A12), (A13), and (A37). In the expansion, the approximation is made that $1 + \zeta_o^2 \simeq 1$ and $I_x \zeta_o$ is small compared to other terms in the equation:

$$M_{exc} = -I_x \ddot{\theta} - c_\theta \dot{\theta} - (I_z - I_y)\Omega^2 \theta - k_\theta \theta - (I_x + I_y - I_z)\Omega \dot{\beta} + (I_z - I_y)\zeta_o \Omega^2 \beta + \zeta_o k_\beta (\beta - \beta_p) \tag{B28}$$

The moment equation (B28) is expressed in the rotating system of the blade (X_r, Y_r) and is now transferred to the gyro axis system (X_c, Y_c). The accompanying sketch (d) shows the three-bladed rotor treated in this development with the rotating frames of the blade (X_r, Y_r) and the gyro (X_c, Y_c).

The moment M_{exc} about the feathering axis of each blade (sketch (d)) will be resolved along the (X_r, Y_r) axis and then transformed to the (X_c, Y_c)

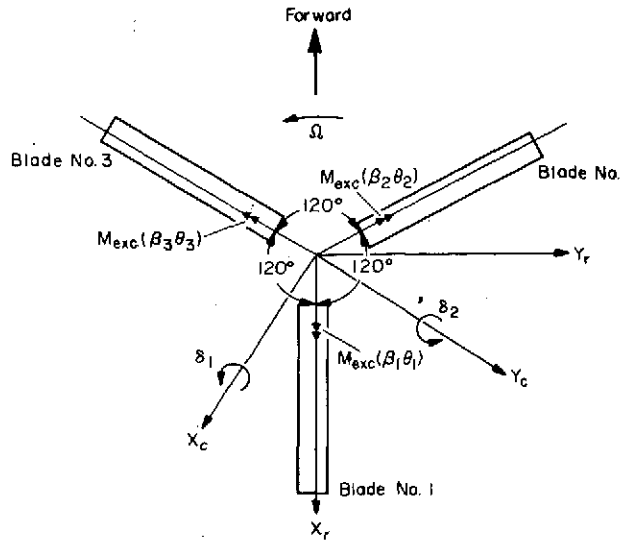

Sketch (d)

axis through a mechanical linkage constant C_2. The excitation of the gyro by the blade is then given by

$$M_{exc_{xc}} = C_2\left[M_{exc}(\beta_1,\theta_1) - \frac{1}{2} M_{exc}(\beta_2,\theta_2) - \frac{1}{2} M_{exc}(\beta_3,\theta_3)\right] \tag{B29}$$

$$M_{exc_{yc}} = C_2\left[\frac{\sqrt{3}}{2} M_{exc}(\beta_2,\theta_2) - \frac{\sqrt{3}}{2} M_{exc}(\beta_3,\theta_3)\right] \tag{B30}$$

Substituting for each moment in equations (B29) and (B30) from (B28) with the appropriate feathering and flapping angles for each of the three blades gives the following moment equations:

$$\begin{aligned} M_{exc_{xc}} = C_2\Big\{ & -I_x\left(\ddot{\theta}_1 - \frac{1}{2}\ddot{\theta}_2 - \frac{1}{2}\ddot{\theta}_3\right) - c_\theta\left(\dot{\theta}_1 - \frac{1}{2}\dot{\theta}_2 - \frac{1}{2}\dot{\theta}_3\right) - (I_z - I_y)\Omega^2\left(\theta_1 - \frac{1}{2}\theta_2 - \frac{1}{2}\theta_3\right) \\ & - k_\theta\left(\theta_1 - \frac{1}{2}\theta_2 - \frac{1}{2}\theta_3\right) - (I_x + I_y - I_z)\Omega\left(\dot{\beta}_1 - \frac{1}{2}\dot{\beta}_2 - \frac{1}{2}\dot{\beta}_3\right) \\ & + (I_z - I_y)\zeta_o\Omega^2\left(\beta_1 - \frac{1}{2}\beta_2 - \frac{1}{2}\beta_3\right) + \zeta_o k_\beta\left[(\beta_1 - \beta_p) - \frac{1}{2}(\beta_2 - \beta_p) - \frac{1}{2}(\beta_3 - \beta_p)\right]\Big\} \end{aligned} \tag{B31}$$

$$M_{exc_{yc}} = \frac{\sqrt{3}}{2} C_2\{-I_x(\ddot{\theta}_2-\ddot{\theta}_3)-c_\theta(\dot{\theta}_2-\dot{\theta}_3)-(I_z-I_y)\Omega^2(\theta_2-\theta_3)-k_\theta(\theta_2-\theta_3)$$

$$-(I_x+I_y-I_z)\Omega(\dot{\beta}_2-\dot{\beta}_3)+(I_z-I_y)\zeta_o\Omega^2(\beta_2-\beta_3)+\zeta_o k_\beta[(\beta_2-\beta_p)-(\beta_3-\beta_p)]\} \tag{B32}$$

The feathering angle θ_i (i = 1,2,3) and its derivatives are now written in terms of the gyro coordinates δ_i (i = 1,2). The relationship between θ_i and δ_i and the derivatives can be obtained from equation (A40). Applying this transformation to equations (B31) and (B32) gives the excitation of the gyro by the blades in gyro coordinates as:

$$M_{exc_{xc}} = -\frac{3}{2} C_2^2 I_x \ddot{\delta}_1 - \frac{3}{2} c_\theta C_2^2 \dot{\delta}_1 - \frac{3}{2} C_2^2 (I_z-I_y)\Omega^2\delta_1 - \frac{3}{2} k_\theta C_2^2 \delta_1$$

$$-C_2(I_x+I_y-I_z)\Omega\left(\dot{\beta}_1-\frac{1}{2}\dot{\beta}_2-\frac{1}{2}\dot{\beta}_3\right)+C_2(I_z-I_y)\zeta_o\Omega^2\left(\beta_1-\frac{1}{2}\beta_2-\frac{1}{2}\beta_3\right)$$

$$+C_2 k_\beta\left[(\beta_1-\beta_p)-\frac{1}{2}(\beta_2-\beta_p)-\frac{1}{2}(\beta_3-\beta_p)\right] \tag{B33}$$

$$M_{exc_{yc}} = -\frac{3}{2} C_2^2 I_x \ddot{\delta}_2 - \frac{3}{2} c_\theta C_2^2 \delta_2 - \frac{3}{2} C_2^2 (I_z-I_y)\Omega^2\delta_2 - \frac{3}{2} k_\theta C_2^2 \delta_2$$

$$-\frac{\sqrt{3}}{2} C_2(I_x+I_y-I_z)\Omega(\dot{\beta}_2-\dot{\beta}_3)+\frac{\sqrt{3}}{2} C_2(I_z-I_y)\zeta_o\Omega^2(\beta_2-\beta_3)$$

$$+\frac{\sqrt{3}}{2} C_2 k_\beta[(\beta_2-\beta_p)-(\beta_3-\beta_p)] \tag{B34}$$

Equations (B33) and (B34) are combined with equations (B25) and (B26) to produce the complete gyro equations for a three-bladed rotor:

$$\left(I_G+\frac{3}{2}C_2^2 I_x\right)\ddot{\delta}_1+\frac{3}{2}c_\theta C_2^2\dot{\delta}_1+C_s\dot{\delta}_1+(I_3\Omega^2 k_R-I_G\Omega^2)\delta_1+\frac{3}{2}C_2^2(I_z-I_y)\Omega^2\delta_1+\frac{3}{2}k_\theta C_2^2\delta_1+K_s\delta_1$$

$$+(I_3\Omega k_R-2\Omega I_G)\dot{\delta}_2-\Omega C_s\delta_2+C_2(I_x+I_y-I_z)\Omega\left(\dot{\beta}_1-\frac{1}{2}\dot{\beta}_2-\frac{1}{2}\dot{\beta}_3\right)-C_2(I_z-I_y)\zeta_o\Omega^2$$

$$\times\left(\beta_1-\frac{1}{2}\beta_2-\frac{1}{2}\beta_3\right)-C_2\zeta_o k_\beta\left[(\beta_1-\beta_p)-\frac{1}{2}(\beta_2-\beta_p)-\frac{1}{2}(\beta_3-\beta_p)\right]$$

$$= \nu_1\sin(\psi+\psi_o)-\nu_2\cos(\psi+\psi_o) \tag{B35}$$

$$\left(I_G+\frac{3}{2}C_2^2I_x\right)\ddot{\delta}_2+\frac{3}{2}c_\theta C_2^2\dot{\delta}_2+C_s\dot{\delta}_2+(I_3\Omega^2k_R-\Omega^2I_G)\delta_2+\frac{3}{2}C_2^2(I_z-I_y)\Omega^2\delta_2+\frac{3}{2}k_\theta C_2^2\delta_2+K_s\delta_2$$

$$-(I_3\Omega k_R-2\Omega I_G)\dot{\delta}_1+\Omega C_s\delta_1+\frac{\sqrt{3}}{2}C_2(I_x+I_y-I_z)\Omega(\dot{\beta}_2-\dot{\beta}_3)-\frac{\sqrt{3}}{2}C_2(I_z-I_y)\zeta_o\Omega^2(\beta_2-\beta_3)$$

$$-\frac{\sqrt{3}}{2}C_2\zeta_o k_\beta[(\beta_2-\beta_p)-(\beta_3-\beta_p)]=\nu_1\cos(\psi+\psi_o)+\nu_2\sin(\psi+\psi_o) \qquad \text{(B36)}$$

APPENDIX C

HUB MOMENT CALCULATIONS FROM MEASURED DATA

This appendix develops the transformations necessary to change the measured shaft bending moments and load cell moments to moments at the hub. The shaft bending moments and load cell moments were measured during wind-tunnel testing at some distance below the hub; the moments obtained from the math model simulation were calculated at the hub. Therefore, it was necessary to transfer the measured moments to the hub in order to have a common point of comparison between measurement and simulation. The coordinate system used to calculate the hub moments is shown in sketch (e).

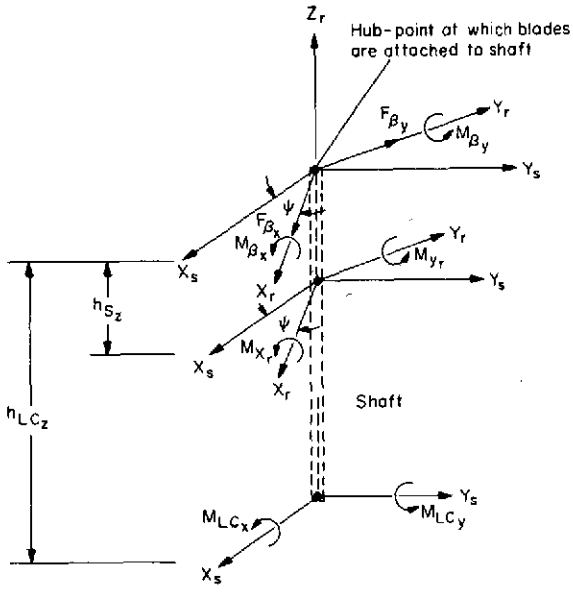

Sketch (e)

The load cell moments were measured in stationary coordinates a distance h_{LC_z} below the hub, while the shaft moments were measured in rotating coordinates a distance h_{S_z} below the hub. In calculating the moments at the hub in rotating coordinates, the following notation and positive direction of moments are adopted:

$$\bar{M}^R_{LC} = \begin{bmatrix} M_{LC_x} \\ M_{LC_y} \end{bmatrix}^{\text{rotating}} = \begin{bmatrix} \text{load cell roll moment (positive left roll)} \\ \text{load cell pitch moment (positive nose-up)} \end{bmatrix} \quad \text{(C1)}$$

$$\bar{M}^R_S = \begin{bmatrix} M_{x_r} \\ M_{y_r} \end{bmatrix}^{\text{rotating}} = \begin{bmatrix} \text{shaft bending moment (positive left roll)} \\ \text{shaft bending moment (positive nose-up)} \end{bmatrix} \quad \text{(C2)}$$

The desired hub moment in rotating coordinates is defined as

$$\bar{M}_{\beta}^{R} = \begin{bmatrix} M_{\beta_x} \\ M_{\beta_y} \end{bmatrix}^{\text{rotating}} = \begin{bmatrix} \text{hub roll moment (positive left roll)} \\ \text{hub pitch moment (positive nose-up)} \end{bmatrix} \tag{C3}$$

The force acting through the hub is defined as

$$\bar{F}_{\beta}^{R} = \begin{bmatrix} F_{\beta_x} \\ F_{\beta_y} \end{bmatrix}^{\text{rotating}} = \begin{bmatrix} \text{hub force along } X_r \\ \text{hub force along } Y_r \end{bmatrix} \tag{C4}$$

The following moment balance can be written from sketch (e):

$$\bar{M}_{LC}^{R} = \bar{M}_{\beta}^{R} + \bar{h}_{LC} \times \bar{F}_{\beta}^{R} \tag{C5}$$

$$\bar{M}_{s}^{R} = \bar{M}_{\beta}^{R} + \bar{h}_{s} \times \bar{F}_{\beta}^{R} \tag{C6}$$

Equations (C5) and (C6) can be solved simultaneously for the moments at the hub from the known measurements of $\bar{M}_{LC}^{R}$, $\bar{M}_{s}^{R}$, $\bar{h}_{LC}$, and $\bar{h}_{s}$. The hub moments are then given by

$$M_{\beta_x} = \frac{h_{LC_z} M_{x_r} - h_{s_z} M_{LC_x}}{h_{LC_z} - h_{s_z}} \tag{C7}$$

$$M_{\beta_y} = \frac{h_{LC_z} M_{y_r} - h_{s_z} M_{LC_y}}{h_{LC_z} - h_{s_z}} \tag{C8}$$

The load cell moments expressed in equations (C7) and (C8) are in the rotating coordinate system. Since the measured load cell moments were recorded in stationary coordinates, the transformation between the rotating and stationary coordinate system must be obtained. This transformation, as indicated in sketch (e), is given as

$$\begin{bmatrix} \bar{r}_1 \\ \bar{r}_2 \\ \bar{r}_3 \end{bmatrix} = \begin{bmatrix} \cos\psi & \sin\psi & 0 \\ -\sin\psi & \cos\psi & 0 \\ 0 & 0 & 1 \end{bmatrix} \begin{bmatrix} \bar{s}_1 \\ \bar{s}_2 \\ \bar{s}_3 \end{bmatrix} \tag{C9}$$

Applying the transformation given by equation (C9) to the M_{LC_x} and M_{LC_y} terms in equations (C7) and (C8) produces the final form of the hub moments in terms of the measured moments:

$$M_{\beta_x} = \frac{h_{LC_z} M_{x_r} - h_{s_z}(M_{LC_x} \cos \psi + M_{LC_y} \sin \psi)}{h_{LC_z} - h_{s_z}} \qquad \text{(C10)}$$

$$M_{\beta_y} = \frac{h_{LC_z} M_{y_r} - h_{s_z}(-M_{LC_x} \sin \psi + M_{LC_y} \cos \psi)}{h_{LC_z} - h_{s_z}} \qquad \text{(C11)}$$

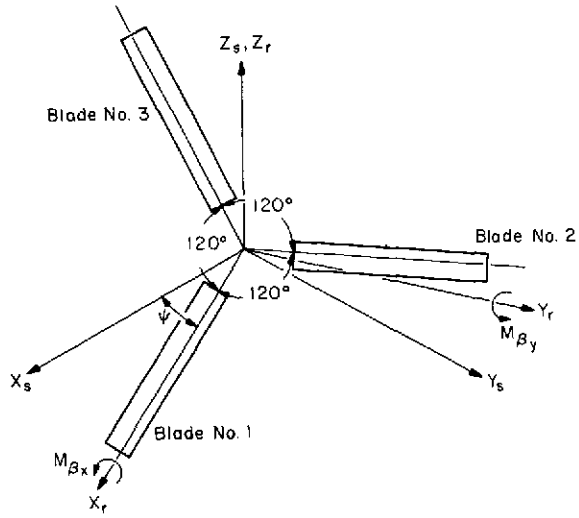

Sketch (f)

In the mathematical model simulation of the rotor, the hub moments were calculated from the blade flapping angles and blade spring constant. Sketch (f) shows the coordinates used to obtain the hub moments in the rotating coordinate system. From the geometric location of the blades for a three-bladed rotor, the hub moments are expressed as

$$M_{\beta_x} = k_\beta \left(\frac{\sqrt{3}}{2} \beta_2 - \frac{\sqrt{3}}{2} \beta_3 \right) \qquad \text{(C12)}$$

$$M_{\beta_y} = k_\beta \left(-\beta_1 + \frac{1}{2} \beta_2 + \frac{1}{2} \beta_3 \right) \qquad \text{(C13)}$$

The calculated hub moments given by equations (C12) and (C13) were then compared with the measured hub moments expressed by equations (C10) and (C11).

REFERENCES

1. Denery, Dallas G.: Identification of System Parameters from Input-Output Data with Application to Air Vehicles. NASA TN D-6468, 1971.

2. Mehra, R. K.; Stepner, D. E.; and Tyler, J. S.: A Generalized Method for the Identification of Aircraft Stability and Control Derivatives from Flight Test Data. Proceedings of Joint Automatic Control Conference, Aug. 1972.

3. Wingrove, R. C.: Quasi-Linearization Technique for Estimating Aircraft States from Flight Data. Journal of Aircraft, vol. 10, no. 5, May 1973.

4. Molusis, J. A.: Helicopter Stability Derivative Extraction from Flight Data Using the Bayesian Approach to Estimation. J. Amer. Helicopter Soc., vol. 18, no. 2, April 1973.

5. Hohenemser, K. H.: and Prelewicz, D. A.: Computer Experiments on Periodic Systems Identification Using Rotor Blade Transient Flapping-Torsion Responses at High Advance Ratio. Specialists Meeting on Rotorcraft Dynamics, American Helicopter Society and NASA/Ames Research Center, Moffett Field, Calif., Feb. 13-15, 1974.

6. Watts, G. A.; London, R. Y.; and Snoddy, R. J.: Trim Control and Stability of a Gyro-Stabilized Hingeless Rotor at High Advance Ratio and Low Rotor Speed. NASA CR-11432, 1971.

7. Watts, G. A.; and Biggers, J. C.: Horizontal Stoppable Rotor Conversion. Presented at 27th Annual Forum of American Helicopter Society, Washington, D.C., Preprint 502, May 1971.

8. Watts, G. A.; and Biggers, J. C.: Hingeless Rotor Vibration and Loads at High Advance Ratio. American Helicopter Society at Mid-East Region Symposium on Status of Testing and Modeling Techniques for V/STOL, Essington, Penn., Oct. 26-28, 1972.

9. Aubrun, Jean-Noel: Nonlinear Systems Identification in Presence of Non-uniqueness. NASA TN D-6467, 1971.

10. Greenwood, Donald Y.: Principles of Dynamics. Prentice-Hall, Inc., Englewood Cliffs, New Jersey, 1965, p. 364.

11. Hall, W. E., Jr.: Application of Floquet Theory to the Analysis of Rotary-Wing VTOL Stability. Stanford Univ. SUDAAR 400, Feb. 1970.

12. Gessow, A.; and Myers, G. D., Jr.: Aerodynamics of the Helicopter. Frederic Ungar Pub. Co., New York, 1967.

13. Sissingh, G. Y.: Response Characteristics of the Gyro-Controlled Lockheed Rotor System. 23rd National Forum of the American Helicopter Society, Washington, D.C., May 1967.

TABLE I.– ROTOR EQUATIONS IN STATE SPACE FORM

$$
\begin{bmatrix} \dot{x}_1 \\ \dot{x}_2 \\ \dot{x}_3 \\ \dot{x}_4 \\ \dot{x}_5 \\ \dot{x}_6 \\ \dot{x}_7 \\ \dot{x}_8 \\ \dot{x}_9 \\ \dot{x}_{10} \end{bmatrix} =
\begin{bmatrix}
0 & 1 & 0 & 0 & 0 & 0 & 0 & 0 & 0 & 0 \\
\frac{-(I_3k_R-I_Q)n^2-\frac{3}{2}c_0^2(I_z-I_y)n^2-\frac{3}{2}k_\beta c_0^2-K_\beta}{I_{GE}} & -\frac{\frac{3}{2}c_0^2-C_\beta}{I_{GE}} & \frac{nC_\beta}{I_{GE}} & -\frac{(I_3k_R-2I_Q)n}{I_{GE}} & \frac{c_0k_\beta+c_2(I_z-I_y)c_0n^2}{I_{GE}} & -\frac{c_2(I_x+I_y-I_z)n}{I_{GE}} & -\frac{\frac{1}{2}c_2c_0k_\beta-\frac{1}{2}c_2(I_z-I_y)c_0n^2}{I_{GE}} & -\frac{\frac{1}{2}c_2(I_x+I_y-I_z)n}{I_{GE}} & 0 & 0 \\
0 & 0 & 0 & 1 & 0 & 0 & 0 & 0 & 0 & 0 \\
\frac{nC_\beta}{I_{GE}} & \frac{(I_3k_R-2I_Q)n}{I_{GE}} & \frac{-(I_3k_Q-I_Q)n^2-\frac{3}{2}c_0^2(I_z-I_y)n^2-\frac{3}{2}k_\beta c_0^2-K_\beta}{I_{GE}} & -\frac{\frac{3}{2}c_0^2-C_\beta}{I_{GE}} & 0 & 0 & \frac{\sqrt{3}}{2}\frac{c_2c_0k_\beta+\frac{\sqrt{3}}{2}c_2(I_z-I_y)c_0n^2}{I_{GE}} & -\frac{\frac{\sqrt{3}}{2}c_2(I_x+I_y-I_z)n}{I_{GE}} & 0 & 0 \\
0 & 0 & 0 & 0 & 0 & 1 & 0 & 0 & 0 & 0 \\
\frac{\frac{1}{2}c_2\gamma n^2\left[B4+2\mu(\zeta_0\cos\psi+\sin\psi)B3+\mu^2\left(\frac{1}{2}-\frac{1}{2}\cos 2\psi+\zeta_0\sin 2\psi\right)B2\right]+\frac{c_2(I_z-I_y)\zeta_0n^2}{I_y}}{} & \frac{c_2(I_x+I_y-I_z)n}{I_y} & 0 & 0 & -\frac{1}{2}\gamma n^2[\zeta_0B4+\mu(\cos\psi+\zeta_0\sin\psi)B3]+\frac{1}{2}\mu^2[\zeta_0+\zeta_0\cos 2\psi+\sin 2\psi)B2]+\frac{1}{2}\gamma n^2\left[B4+2\mu(\zeta_0\cos\psi+\sin\psi)B3+\mu^2\left(\frac{1}{2}-\frac{1}{2}\cos 2\psi+\zeta_0\sin 2\psi\right)B2\right]\tan\delta_3-\frac{k_\beta}{I_y}+\frac{(I_x+I_y\zeta_0^2-I_z)n^2}{I_y}-\frac{\frac{3}{2}eR^2}{R-e} & -\frac{1}{2}\gamma n^2\left[\frac{B4}{n}+\frac{\mu}{n}(\zeta_0\cos\psi+\sin\psi)B3\right] & 0 & 0 & 0 & 0 \\
0 & 0 & 0 & 0 & 0 & 0 & 0 & 0 & 1 & 0 \\
-\frac{1}{4}c_2\gamma n^2\left\{B4+2\mu[\zeta_0\cos(\psi+120°)+\sin(\psi+120°)]B3+\mu^2\left[\frac{1}{2}-\frac{1}{2}\cos 2(\psi+120°)+\zeta_0\sin 2(\psi+120°)\right]B2\right\}-\frac{\frac{1}{2}c_2(I_z-I_y)\zeta_0n^2}{I_y} & -\frac{\frac{1}{2}nC_2(I_x+I_y-I_z)}{I_y} & \frac{\sqrt{3}}{4}c_2\gamma n^2\left\{B4+2\mu[\zeta_0\cos(\psi+120°)+\sin(\psi+120°)]B3+\mu^2\left[\frac{1}{2}-\frac{1}{2}\cos 2(\psi+120°)+\zeta_0\sin 2(\psi+120°)\right]B2\right\}+\frac{\frac{\sqrt{3}}{2}c_2(I_z-I_y)\zeta_0n^2}{I_y} & \frac{\sqrt{3}}{2}\frac{nC_2(I_x+I_y-I_z)}{I_y} & -\frac{1}{2}\gamma n^2\{\zeta_0B4+\mu[\cos(\psi+120°)+\zeta_0\sin(\psi+120°)]B3+\frac{1}{2}\mu^2[\zeta_0+\zeta_0\cos 2(\psi+120°)+\sin 2(\psi+120°)]B2)+\frac{1}{2}\gamma n^2\left\{B4+2\mu[\zeta_0\cos(\psi+120°)+\sin(\psi+120°)]B3+\mu^2\left[\frac{1}{2}-\frac{1}{2}\cos 2(\psi+120°)+\zeta_0\sin 2(\psi+120°)\right]B2\right\}\tan\delta_3-\frac{k_\beta}{I_y}+\frac{(I_x+I_y\zeta_0^2-I_z)n^2}{I_y}-\frac{\frac{3}{2}eR^2}{R-e} & -\frac{1}{2}\gamma n^2\left\{\frac{B4}{n}+\frac{\mu}{n}[\zeta_0\cos(\psi+120°)+\sin(\psi+120°)]B3\right\} & 0 & 0 & 0 & 0 \\
0 & 0 & 0 & 0 & 0 & 0 & 0 & 0 & 0 & 1 \\
-\frac{1}{4}c_2\gamma n^2\left\{B4+2\mu[\zeta_0\cos(\psi+240°)+\sin(\psi+240°)]B3+\mu^2\left[\frac{1}{2}-\frac{1}{2}\cos 2(\psi+240°)+\zeta_0\sin 2(\psi+240°)\right]B2\right\}-\frac{\frac{1}{2}c_2(I_z-I_y)\zeta_0n^2}{I_y} & -\frac{\frac{1}{2}nC_2(I_x+I_y-I_z)}{I_y} & -\frac{\sqrt{3}}{4}c_2\gamma n^2\left\{B4+2\mu[\zeta_0\cos(\psi+240°)+\sin(\psi+240°)]B3+\mu^2\left[\frac{1}{2}-\frac{1}{2}\cos 2(\psi+240°)+\zeta_0\sin 2(\psi+240°)\right]B2\right\}-\frac{\frac{\sqrt{3}}{2}c_2(I_z-I_y)\zeta_0n^2}{I_y} & -\frac{\sqrt{3}}{2}\frac{nC_2(I_x+I_y-I_z)}{I_y} & -\frac{1}{2}\gamma n^2\left\{\zeta_0B4+\mu[\cos(\psi+240°)+\zeta_0\sin(\psi+240°)]B3+\frac{1}{2}\mu^2[\zeta_0+\zeta_0\cos 2(\psi+240°)+\sin 2(\psi+240°)]B2\right\}+\frac{1}{2}\gamma n^2\left\{B4+2\mu[\zeta_0\cos(\psi+240°)+\sin(\psi+240°)]B3+\mu^2\left[\frac{1}{2}-\frac{1}{2}\cos 2(\psi+240°)+\zeta_0\sin 2(\psi+240°)\right]B2\right\}\tan\delta_3-\frac{k_\beta}{I_y}+\frac{(I_x+I_y\zeta_0^2-I_z)n^2}{I_y}-\frac{\frac{3}{2}eR^2}{R-e} & -\frac{1}{2}\gamma n^2\left\{\frac{B4}{n}+\frac{\mu}{n}[\zeta_0\cos(\psi+240°)+\sin(\psi+240°)]B3\right\} & 0 & 0 & 0 & 0
\end{bmatrix}
\begin{bmatrix} x_1 \\ x_2 \\ x_3 \\ x_4 \\ x_5 \\ x_6 \\ x_7 \\ x_8 \\ x_9 \\ x_{10} \end{bmatrix}
+
\begin{bmatrix}
0 \\
\frac{\nu_1}{I_{GE}}\sin(\psi+\psi_0)-\frac{\nu_2}{I_{GE}}\cos(\psi+\psi_0) \\
0 \\
\frac{\nu_1}{I_{GE}}\cos(\psi+\psi_0)+\frac{\nu_2}{I_{GE}}\sin(\psi+\psi_0) \\
0 \\
\frac{1}{2}\gamma n^2\left[B4+2\mu(\zeta_0\cos\psi+\sin\psi)B3+\mu^2\left(\frac{1}{2}-\frac{1}{2}\cos 2\psi+\zeta_0\sin 2\psi\right)B2\right]\theta_0+\frac{1}{2}\gamma n^2\left[B5+2\mu(\zeta_0\cos\psi+\sin\psi)B4+\mu^2\left(\frac{1}{2}-\frac{1}{2}\cos 2\psi+\zeta_0\sin 2\psi\right)B3\right]\theta_1+\frac{1}{2}\gamma n^2[B3+\mu(\zeta_0\cos\psi+\sin\psi)B2]\lambda_0+\frac{1}{2}\gamma n^2[B4\cos\psi+\mu(\cos\psi\sin\psi+\zeta_0\cos^2\psi)B3]\lambda_x+\frac{1}{2}\gamma n^2[B4\sin\psi+\mu(\sin^2\psi+\zeta_0\cos\psi\sin\psi)B3]\lambda_y+\frac{k_\beta}{I_y}\beta_p \\
0 \\
\frac{1}{2}\gamma n^2\left\{B4+2\mu[\zeta_0\cos(\psi+120°)+\sin(\psi+120°)]B3+\mu^2\left[\frac{1}{2}-\frac{1}{2}\cos 2(\psi+120°)+\zeta_0\sin 2(\psi+120°)\right]B2\right\}\theta_0+\frac{1}{2}\gamma n^2\left\{B5+2\mu[\zeta_0\cos(\psi+120°)+\sin(\psi+120°)]B4+\mu^2\left[\frac{1}{2}-\frac{1}{2}\cos 2(\psi+120°)+\zeta_0\sin 2(\psi+120°)\right]B3\right\}\theta_1+\frac{1}{2}\gamma n^2[B3+\mu[\zeta_0\cos(\psi+120°)+\sin(\psi+120°)]B2]\lambda_0+\frac{1}{2}\gamma n^2[B4\cos(\psi+120°)+\mu[\cos(\psi+120°)\sin(\psi+120°)+\zeta_0\cos^2(\psi+120°)]B3]\lambda_x+\frac{1}{2}\gamma n^2[B4\sin(\psi+120°)+\mu[\sin^2(\psi+120°)+\zeta_0\cos(\psi+120°)\sin(\psi+120°)]B3]\lambda_y+\frac{k_\beta}{I_y}\beta_p \\
0 \\
\frac{1}{2}\gamma n^2\left\{B4+2\mu[\zeta_0\cos(\psi+240°)+\sin(\psi+240°)]B3+\mu^2\left[\frac{1}{2}-\frac{1}{2}\cos 2(\psi+240°)+\zeta_0\sin 2(\psi+240°)\right]B2\right\}\theta_0+\frac{1}{2}\gamma n^2\left\{B5+2\mu[\zeta_0\cos(\psi+240°)+\sin(\psi+240°)]B4+\mu^2\left[\frac{1}{2}-\frac{1}{2}\cos 2(\psi+240°)+\zeta_0\sin 2(\psi+240°)\right]B3\right\}\theta_1+\frac{1}{2}\gamma n^2[B3+\mu[\zeta_0\cos(\psi+240°)+\sin(\psi+240°)]B2]\lambda_0+\frac{1}{2}\gamma n^2[B4\cos(\psi+240°)+\mu[\cos(\psi+240°)\sin(\psi+240°)+\zeta_0\cos^2(\psi+240°)]B3]\lambda_x+\frac{1}{2}\gamma n^2[B4\sin(\psi+240°)+\mu[\sin^2(\psi+240°)+\zeta_0\cos(\psi+240°)\sin(\psi+240°)]B3]\lambda_y+\frac{k_\beta}{I_y}\beta_p
\end{bmatrix}
$$

$$
\begin{bmatrix} y_1 \\ y_2 \end{bmatrix} =
\begin{bmatrix} 0 & +\frac{\sqrt{3}}{2}k_\beta & -\frac{\sqrt{3}}{2}k_\beta \\ -k_\beta & +\frac{1}{2}k_\beta & +\frac{1}{2}k_\beta \end{bmatrix}
\begin{bmatrix} x_5 \\ x_7 \\ x_9 \end{bmatrix}
$$

TABLE 2.- ROTOR AND GYRO PARAMETERS

Parameters	Nominal values with allowed percentage variation
Rotor:	
Number of blades (b)	3
Blade inertia (for each of b blades)	
Feathering inertia (I_x)	0.54 kg-m^2 (0.4 slug-ft^2)
Flapping inertia (I_y)	363.4 kg-m^2 (268 slug-ft^2) ± 1 percent
Inplane inertia (I_z)	363.9 kg-m^2 (268.4 slug-ft^2) ± 1 percent
Blade twist (θ_1)	-9.43° ± 5 percent
Collective angle at root (θ_o)	8.57° ± 7 percent
Sweep angle (ζ_o)	1.5° ± 20 percent
Precone angle (β_p)	2.25° ± 5 percent
Tip loss factor (B_ℓ)	0.97 ± 2 percent
Blade radius (R_b)	5.03 m (16.5 ft)
Blade chord width (c)	0.357 m (1.17 ft)
Airfoil type	NACA 63_2015
Solidity	0.0675
Blade area	5.36 m^2 (57.7 ft^2)
Disk area	79.46 m^2 (855.3 ft^2)
Mast angle forward tilt	0°
Rotor RPM (100 percent)	355.6
Hinge offset (e/R_b)	0.11 ± 30 percent
Lock number, $\gamma = \frac{c\rho a R_b^4}{I_y}$	4.57 ± 10 percent
Spring constant (p from fig. 4)	±30 percent
$k_\beta = I_y\Omega^2\left(p^2-1-\frac{(3/2)e}{R-e}-\frac{\gamma}{8}\tan\delta_3\right)$	
Gyro:	
Gyro inertia	
Polar moment of inertia (I_3)	0.41 kg-m^2 (0.3 slug-ft^2) ± 2 percent
Diametric moment of inertia (I_D)	0.21 kg-m^2 (0.15 slug-ft^2) ± 2 percent
Gyro pitch link angle (ψ_o)	60° ± 2 percent
Mechanical advantage constant (C_2)	0.87 ± 3 percent
Gyro RPM (100 percent)	10,000

TABLE 3.- PARAMETER ESTIMATES FOR STEADY-STATE LOCKED GYRO OPERATION

Condition	Parameter	Value	
		Nominal	Estimated
V = 41.2 m/sec (80 knots) μ = 0.399 rpm = 55.5 percent	θ_o	8.57°	7.97
	B_ℓ	0.97	0.95
	C_2	0.87	0.85
	I_y	363.4 kg-m^2 (268 slug-ft^2)	359.7 kg-m^2 (265.3 slug-ft^2)
	I_z	363.9 kg-m^2 (268.4 slug-ft^2)	360.2 kg-m^2 (265.7 slug-ft^2)
	γ	4.67	5.13
	k_β	141,092 Nm/rad (104,064 ft-lb/rad)	129,345 Nm/rad (95,400 ft-lb/rad)
	ζ_o	1.5°	1.6°
	β_p	2.25°	2.36°
	λ_o	-0.012	-0.012 (fixed)
	e/R_b	0.11	0.11
V = 31.3 m/sec (61 knots) μ = 0.402 rpm = 41.6 percent	θ_o	8.57°	7.97°
	B_ℓ	0.97	0.95
	C_2	0.87	0.85
	I_y	363.4 kg-m^2 (268 slug-ft^2)	359.7 kg-m^2 (265.3 slug-ft^2)
	I_z	363.9 kg-m^2 (268.4 slug-ft^2)	360.2 kg-m^2 (265.7 slug-ft^2)
	γ	4.69	5.16
	k_β	125,214 Nm/rad (92,353 ft-lb/rad)	87,651 Nm/rad (64,648 ft-lb/rad)
	ζ_o	1.5°	1.6°
	β_p	2.25°	2.14°
	λ_o	0.005	0.005 (fixed)
	e/R_b	0.11	0.11

TABLE 4.- PARAMETER ESTIMATES FOR TRANSIENT FREE AND LOCKED GYRO OPERATION; V = 36 m/sec (70 knots), μ = 0.355, 54.2 percent rpm

	Condition of gyro	Parameter	Values	
			Nominal	Estimated
Parameter cases studied	Free	θ_o	8.57°	9.17°
		θ_1	-9.43°	-10.93°
		B_ℓ	0.97	0.96
		γ	4.57	4.0
		k_β	138,752 Nm/rad (102,338 ft-lb/rad)	97,127 Nm/rad (71,637 ft-lb/rad)
		ζ_o	1.5°	1.8°
	Free	θ_o	8.57°	9.17°
		B_ℓ	0.97	0.98
		I_y	363.4 kg-m^2 (268 slug-ft^2)	366.5 kg-m^2 (270.3 slug-ft^2)
		γ	4.57	4.0
		k_β	138,752 Nm/rad (102,338 ft-lb/rad)	97,127 Nm/rad (71,637 ft-lb/rad)
		ζ_o	1.5°	1.8°
		e/R_b	0.11	0.15
	Locked	θ_o	8.57°	9.17°
		B_ℓ	0.97	0.98
		C_2	0.87	0.85
		I_y	363.4 kg-m^2 (268 slug-ft^2)	359.7 kg-m^2 (265.3 slug-ft^2)
		γ	4.57	5.02
		k_β	138,752 Nm/rad (102,338 ft-lb/rad)	97,795 Nm/rad (72,130 ft-lb/rad)
		μ	0.355	0.348
		ζ_o	1.5°	1.8°
		β_p	2.25°	2.14°
		e/R_b	0.11	0.15

TABLE 5.- SENSITIVITIES OF MODEL PARAMETERS OBTAINED FROM IDENTIFICATION PROGRAM

Parameter	Sensitivity constant
θ_o	4.0
θ_1	3.2
B_ℓ	2.7
C_2	1.1
$\gamma, (I_y, I_z)$	.78
k_β	.75
μ	.72
k_R	.57
I_G	.57
ζ_o	.52
β_p	.31
λ_o	.15
C_s	.13
c_θ	.07
I_x	.03
e	.02

U.S. Government Printing Office: 1974—636-486/33 Region No. 3-II